

Lanthanide-Based Coordination Polymers Assembled by a Flexible Multidentate Linker: Design, Structure, Photophysical Properties, and Dynamic Solid-State Behavior

Claire Marchal,^[a] Yaroslav Filinchuk,^[b] Xiao-Yan Chen,^[a] Daniel Imbert,^[a] and Marinella Mazzanti*^[a]

Abstract: Four picolinate building blocks were implemented into the multidentate linker *N,N',N'*-tetrakis[(6-carboxypyridin-2-yl)methyl]butylenediamine (H₄tpabn) with a linear flexible spacer to promote the assembly of lanthanide-based 1D coordination polymers. The role of the linker in directing the geometry of the final assembly is evidenced by the different results obtained in the presence of Htpabn³⁻ and tpabn⁴⁻ ions. The tpabn⁴⁻ ion leads to the desired 1D polymer {[Nd(tpabn)]H₃O·6H₂O}_∞ (**12**). The

Htpabn³⁻ ion leads to the assembly of Tb^{III} and Er^{III} ions into 1D zigzag chains of the general formula {[M(Htpabn)]·xH₂O}_∞ (M=Tb, x=14 (**1**); M=Tb, x=8 (**11**); M=Er, x=14 (**2**); M=Er, x=5.5 (**4**)), a 2D network is formed by the Eu^{III} ion (i.e., {[Eu(Htpabn)]·10H₂O}_∞ (**7**)), and both supramolecular isomers (1D and 2D)

are obtained by the Tb^{III} ion. The high flexibility of the polymeric chains results in a dynamic behavior with a solvent-induced reversible structural transition. The Tb^{III}- and Eu^{III}-containing polymers display high-luminescence quantum yields (38 and 18%, respectively). A sizeable near-IR luminescence emission is observed for the Er^{III}- and Nd^{III}-containing polymers when lattice water molecules are removed.

Keywords: chromophores • lanthanides • luminescence • polymers • supramolecular chemistry

Introduction

Metal–organic frameworks (MOFs) based on rare-earth metal elements are attracting increasing attention due to their ability to form multifunctional materials that combine desirable structural features with the interesting magnetic, optical, and catalytic properties of the lanthanide ions.^[1–5] Notably, because of their interesting photophysical properties (characteristic sharp emission, long lifetime, large

Stokes shift),^[6] lanthanide-based coordination polymers are excellent candidates for the development of light-emitting diodes^[7] and sensors.^[8] Recently, several lanthanide coordination polymers with interesting photophysical properties, a few of which couple luminescence and porosity, have been reported.^[9–16] However, lanthanide systems remain far less studied than frameworks based on d-block transition-metal elements^[17–20] because the typically unspecific coordination properties of the lanthanide ions render the design of lanthanide-based coordination frameworks with specific properties very challenging. By contrast, the coordination flexibility of lanthanide ions can lead to unusual structural topologies and new framework families.^[3] The majority of the reported lanthanide frameworks are formed by using low-density rigid organic building blocks. Because of the lack of a preferred coordination number or geometry of the lanthanide ions, the final structure remains difficult to predict in such a synthetic approach, thus preventing a systematic investigation of structure–property relations. Moreover, low-density linkers often result in the presence of solvent molecules coordinated to the metal ion that lead to luminescence quenching and low thermal stability.

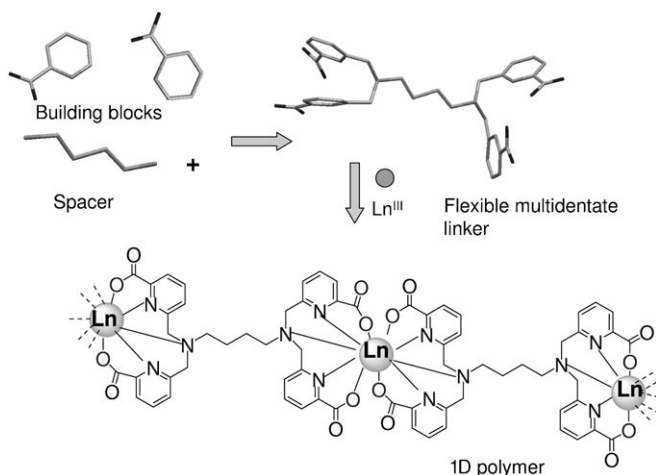
[a] Dr. C. Marchal, Dr. X.-Y. Chen, Dr. D. Imbert, Dr. M. Mazzanti
Laboratoire de Reconnaissance Ionique et Chimie de Coordination
Service de Chimie Inorganique et Biologique (UMR-E 3 CEA-UJF)
CEA/DSM/INAC, CEA-Grenoble
38054 Grenoble, Cedex 09 (France)

[b] Dr. Y. Filinchuk
Swiss–Norwegian Beam Lines (SNBL)
European Synchrotron Radiation Facility (ESRF)
rue Jules Horowitz, 38043 Grenoble (France)

Supporting information for this article is available on the WWW under <http://dx.doi.org/10.1002/chem.200802589>.

The coordination chemistry of lanthanides with multidentate linkers has been investigated in depth to selectively introduce lanthanide ions into monometallic or discrete poly-metallic architectures for the development of water-stable luminescent probes.^[21–24] Significantly enhanced luminescence emission can be achieved by incorporating lanthanide ions into a multidentate linker that contains a suitable building block that can efficiently absorb energy and transfer it to the metal ion (often referred to as the “antenna effect”). Such high-denticity linkers also allow good protection of the metal center from O–H oscillators of coordinated or closely diffusing solvent molecules that would lead to nonradiative deactivation of the lanthanide excited states. Predisposed flexible multidentate ligands in which an anchor ensures that the geometry and orientation of dangling chelating units have been successfully used to carefully control the coordination properties of lanthanide ions in the rational design of monometallic complexes.^[25–29] Particularly relevant is the recent thermodynamic study of Piguet and co-workers that introduces a new tool (the effective concentration) for the quantitative estimation of the preorganization of multidentate linkers, which could be useful in any multicomponent assembly process.^[30] However, flexible multidentate linkers have been rarely used in the construction of lanthanide-based coordination polymers^[31–36] in spite of their expected increased thermal stability, ability to provide insight into supramolecular isomerism or polymorphism, and potential to support structural dynamism in a functional porous framework. This aspect is underdeveloped but crucial in the development of new materials with specificity for molecular recognition.^[17,35–38] Taking advantage of the knowledge acquired with monometallic systems, we have used a new topological approach in which suitable building blocks are implemented into a multidentate linker with a flexible spacer to direct the geometry and dimensionality of lanthanide frameworks (Scheme 1).

Picolinates were chosen as suitable building blocks for the construction of a potential decadentate linker because of



Scheme 1. Ligand design for the assembly of 1D coordination polymers.

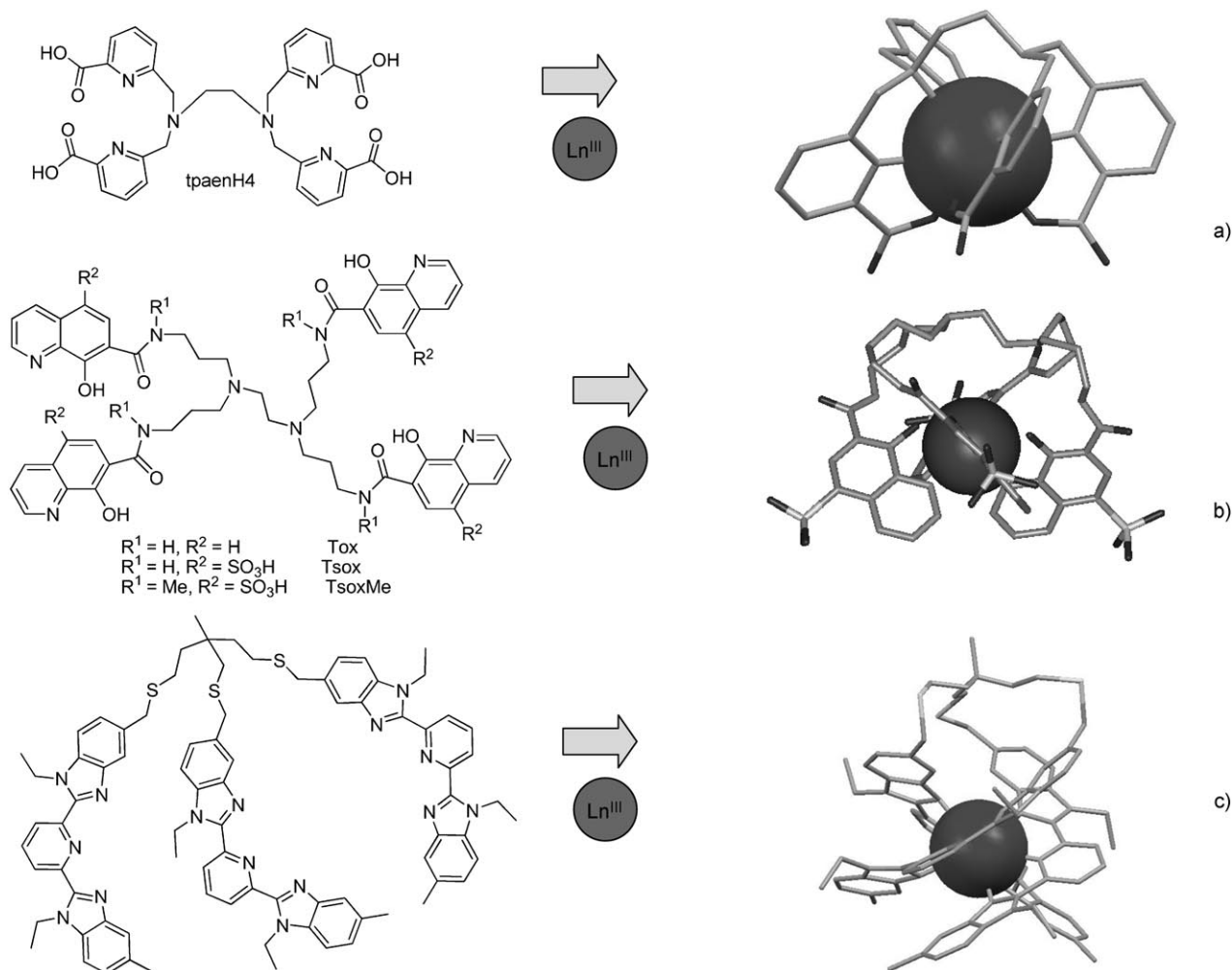
their efficient sensitization of lanthanide ions^[29,40] and their versatile chemistry. Previously, we found that 10^{-2} M solutions of the decadentate tetrapodal ligand tpaen^{4-} ($\text{H}_4\text{tpaen} = \text{N},\text{N},\text{N}',\text{N}'\text{-tetrakis}[(6\text{-carboxypyridin-2-yl)methyl}] \text{ethylenediamine}$), in which four picolinate building blocks are connected by an ethylenediamine spacer, in water react with lanthanide ions to afford only mononuclear ten-coordinate complexes, even in the presence of excess metal (Scheme 2).^[29] Mononuclear complexes can still be obtained when low-denticity binding units (e.g., bidentate^[29,41] or tridentate^[30,41]) are connected to a spacer by highly flexible arms to yield a strain-free multidentate linker (Scheme 2), but the preorganization remains small in some of these systems and polymetallic complexes can form depending on the conditions.^[30]

In this study, a long flexible four-carbon-atom aliphatic spacer was chosen to connect four picolinate building blocks into the potentially decadentate linker tpabn^{4-} ($\text{H}_4\text{tpabn} = \text{N},\text{N},\text{N}',\text{N}'\text{-tetrakis}[(6\text{-carboxypyridin-2-yl)methyl}] \text{butylenediamine}$). The introduction of flexibility at the spacer level rather than in the arms leads to considerably decreased stability of lanthanide monometallic complexes with respect to polymetallic complexes (at least in similar concentrations) by lowering the chelate effect of the multidentate ligands. Moreover, the presence of two distinct potentially pentadentate dianionic dipodal chelating units favors the formation of 1D polymers rather than higher dimensionality networks. In a preliminary study, a highly luminescent 1D polymer of terbium was isolated and structurally characterized. Herein, we describe a complete study of the influence of the linker preorganization and lanthanide size on the structure and dimensionality of the final framework together with a quantitative study of the photophysical properties of the resulting polymers and their dynamic solid-state behavior. We show that the perfect matching of ligand denticity with the requirements of the lanthanide ion leads to a predictable and unique structure that confirms the validity of the chosen topological approach, whereas a lack of ligand predisposition can result in supramolecular isomers that depend on the ion size and synthetic conditions.

Experimental Section

General: The solvents and starting materials were obtained from Aldrich, Fluka, and Acros, and used without further purification unless otherwise stated. Elemental analyses were performed by the Service Central d'Analyses (Vernaison, France) or under a controlled atmosphere of argon by the Pr. Malissa and Reuteur Laboratory (Lindlar, Germany). Thermogravimetric analysis (TGA) experiments were carried out on a Setaram TGA92 analyzer under an argon flow in the range 30–800 °C at a heating rate of 10 °C min⁻¹. The ¹H NMR spectra were recorded on Varian UNITY 400 MHz spectrometer. The NMR chemical shifts are reported in ppm with the solvent as an internal reference.

***N,N,N',N'*-Tetrakis[(6-carboxypyridin-2-yl)methyl]butylenediamine (H_4tpabn):** 1,4-Diaminobutane dihydrochloride (0.497 g, 3.09 mmol), K_2CO_3 (2.90 g, 21.0 mmol), and KI (2.08 g, 12.5 mmol) were successively added to a solution of ethyl 6-chloromethylpyridine-2-carboxylate (2.50 g, 12.5 mmol) in anhydrous acetonitrile (50 mL) under an argon at-


 Scheme 2. Flexible ligands that yield monometallic lanthanide complexes at a) any M/L ratio^[29] or b, c) M/L = 1:1.^[30,44]

mosphere. The reaction mixture was filtered after heating to reflux for 18 h. The solvent was evaporated to afford a yellow oil, which was dissolved in dichloromethane (60 mL). The resulting solution was washed with a saturated NaHCO_3 solution (2×60 mL), dried over anhydrous Na_2SO_4 , filtered, and evaporated to dryness to give a yellow oil that was purified by flash chromatography on neutral aluminum oxide (230 mL, $\text{CH}_2\text{Cl}_2/\text{EtOH}$ gradient from 99.5:0.5 to 98:2). The product (1.26 g, 1.70 mmol) was heated to reflux overnight in a 6 M HCl solution (50 mL). After concentration of the solvent to approximately 5 mL, the solution was stored at 5°C. The obtained white solid was filtered, washed with cold water, and dried under vacuum to yield $\text{H}_4\text{tpabn} \cdot 2\text{HCl} \cdot \text{H}_2\text{O}$ (0.85 g, 39%). $^1\text{H NMR}$ (D_2O , 400 MHz, 298 K, $\text{pD} = 6.3$): $\delta = 1.91$ (s, 4H; $-\text{CH}_2\text{CH}_2-$), 3.32 (s, 4H; NCH_2), 4.46 (s, 8H; NCH_2py), 7.27 (m, 4H; H_4), 7.65 ppm (m, 8H; H_3, H_5); $^{13}\text{C NMR}$ (D_2O , 400 MHz, 298 K, $\text{pD} = 6.3$): $\delta = 22.2$ (CH_2), 56.4 (CH_2), 59.6 (CH_2), 124.1 (CHpy), 126.2 (CHpy), 138.4 (CHpy), 149.8 (Cpy), 153.1 (Cpy), 172.3 ppm (COOH); elemental analysis (%) calcd for $\text{C}_{32}\text{H}_{36}\text{N}_6\text{O}_9\text{Cl}_2$: C 53.41, H 5.04, N 11.63; found: C 53.20, H 4.98, N 11.55.

Coordination polymer synthesis

$\{[\text{Ln}(\text{Htpabn})] \cdot x\text{H}_2\text{O}\}_\infty$: A solution of $\text{LnCl}_3 \cdot 6\text{H}_2\text{O}$ ($\text{Ln} = \text{Tb}, \text{Er}$; 0.05 mmol) in EtOH/water (4:1; 5 mL) was allowed to slowly diffuse into a solution of $\text{LnCl}_3 \cdot 6\text{H}_2\text{O}$ (0.05 mmol) and H_4tpabn (0.10 mmol) in water (9.0 mL) at pH 6.5 (adjusted by the addition of Et_3N). The formation of small crystals of $\{[\text{Ln}(\text{Htpabn})] \cdot 14\text{H}_2\text{O}\}_\infty$ ($\text{Ln} = \text{Tb}^{\text{III}}$ (**1**); Er^{III} (**2**)) suitable for X-ray diffraction studies was observed within a few days. The crystals were filtered, washed with water, and dried under vacuum for a

few minutes to yield the Tb^{III} - and Er^{III} -containing polymers $\{[\text{Tb}(\text{Htpabn})] \cdot 5.5\text{H}_2\text{O}\}_\infty$ (**3**) and $\{[\text{Er}(\text{Htpabn})] \cdot 5.5\text{H}_2\text{O}\}_\infty$ (**4**) as white and pale-pink crystalline powders, respectively (58–60% yield). **3**: Elemental analysis (%) calcd for $\text{C}_{32}\text{H}_{40}\text{N}_6\text{O}_{13.5}\text{Tb}$: C 43.50, H 4.56, N 9.51; found: C 43.10, H 4.52; N 9.49. **4**: Elemental analysis (%) calcd for $\text{C}_{32}\text{H}_{40}\text{N}_6\text{O}_{13.5}\text{Er}$: C 43.09, H 4.52, N 9.42; found: C 43.02, H 4.37, N 9.31. Both **3** and **4** display the same powder X-ray diffraction (PXRD) patterns consistent with the calculated patterns, thus confirming the identity and phase purity of the two polymers.

Slow evaporation of a small portion of the solution containing the crystals of Er^{III} complex **2** resulted in the isolation of crystals of the partially hydrated compound $\{[\text{Er}(\text{Htpabn})] \cdot 5.5\text{H}_2\text{O}\}_\infty$ (**4**) suitable for X-ray diffraction studies.

The TGA of complex $\{[\text{Tb}(\text{Htpabn})] \cdot 5.5\text{H}_2\text{O}\}_\infty$ displayed a first weight loss of 12.16% between 30 and 110°C, which corresponds to the loss of 5.5 guest water molecules (calcd: 12.10%). Decomposition of the complex started above 250°C (see Figure S1 in the Supporting Information).

All the guest water molecules can be removed by drying the polymers under vacuum at 130°C for six days to obtain the dry Er^{III} - and Tb^{III} -containing polymers $[\text{Tb}(\text{Htpabn})]_\infty$ (**5**) and $[\text{Er}(\text{Htpabn})]_\infty$ (**6**). **5**: Elemental analysis (%) calcd for $\text{C}_{32}\text{H}_{29}\text{N}_6\text{O}_8\text{Tb}$: C 48.99, H 3.73, N 10.71; found: C 48.90, H 3.81, N 10.73. **6**: Elemental analysis (%) calcd for $\text{C}_{32}\text{H}_{29}\text{N}_6\text{O}_8\text{Er}$: C 48.48, H 3.69, N 10.60; found: C 48.23, H 3.59, N 10.38.

Synthesis of $\{[\text{Eu}(\text{Htpabn})] \cdot x\text{H}_2\text{O}\}_\infty$: A solution of $\text{EuCl}_3 \cdot 6\text{H}_2\text{O}$ (0.069 mmol) in water (5 mL) was allowed to slowly diffuse into a solu-

tion of $\text{EuCl}_3 \cdot 6\text{H}_2\text{O}$ (0.069 mmol) and H_4tpabn (0.138 mmol) in water (9.0 mL) at pH 6.5 (adjusted by the addition of a 0.1 M solution of KOH). Some small crystals suitable for X-ray diffraction studies appeared after two weeks. X-ray diffraction analysis performed on the crystals transferred directly from the mother liquor to paraton oil showed the presence of $\{[\text{Eu}(\text{Htpabn})] \cdot 10\text{H}_2\text{O}\}_\infty$ (**7**). The remaining crystals were filtered, washed with water, and dried under vacuum for a few minutes to yield the dehydrated Eu^{III} -containing polymer $\{[\text{Eu}(\text{Htpabn})] \cdot 8.5\text{H}_2\text{O}\}_\infty$ (**8**) as a white crystalline powder (66%). Elemental analysis (%) calcd for $\text{C}_{32}\text{H}_{46}\text{N}_6\text{O}_{16.5}\text{Eu}$: C 41.30, H 4.98, N 9.03; found: C, 41.33, H 4.54; N 9.10.

The synthesis of the Eu-containing polymer was also performed in the presence of triethylamine as a base. The powder obtained displayed a very different PXRD pattern. An automatic indexing was attempted by DicVol04. Five monoclinic solutions were found, but it was not possible to determine this new structure.

The TGA of **8** showed the first weight loss of 6.50% between 30 and 110°C, which corresponds to the loss of 3.5 water molecules (calcd: 6.77%). No further loss was observed until the decomposition of the complex, which started above 250°C (see Figure S2 in the Supporting Information).

The guest water molecules could be partially removed by drying the crystals under vacuum at 130°C for six days to obtain the partially hydrated Eu^{III} -containing polymer $\{[\text{Eu}(\text{Htpabn})] \cdot 5\text{H}_2\text{O}\}_\infty$ (**9**). Elemental analysis (%) calcd for $\text{C}_{32}\text{H}_{39}\text{N}_6\text{O}_{13}\text{Eu}$: C 44.30, H 4.53, N 9.69; found: C 44.42, H 4.73, N 10.04.

Crystals of the 2D polymer $\{[\text{Tb}(\text{Htpabn})] \cdot 10\text{H}_2\text{O}\}_\infty$ (**10**) were isolated when a solution of $\text{TbCl}_3 \cdot 6\text{H}_2\text{O}$ (7.0 μmol) in water (0.5 mL) was allowed to slowly diffuse into a solution of $\text{TbCl}_3 \cdot 6\text{H}_2\text{O}$ (7.0 μmol) and H_4tpabn (0.14 mmol) in water (1 mL) at pH 6.5 (adjusted by the addition of a 0.1 M solution of KOH). However, a large-scale synthesis of the Tb-containing polymer in the same base (KOH) and under the same concentration conditions led to the isolation of crystals of the 1D polymer $\{[\text{Tb}(\text{Htpabn})] \cdot 8\text{H}_2\text{O}\}_\infty$ (**11**). The PXRD data on the bulk isolated material indicated that the 1D polymer was the only detectable compound.

Synthesis of $\{[\text{Nd}(\text{tpabn})] \cdot 6\text{H}_2\text{O}\}_\infty$: A solution of $\text{NdCl}_3 \cdot 6\text{H}_2\text{O}$ (0.050 mmol) in EtOH/water (4:1, 5 mL) was allowed to slowly diffuse into a solution of $\text{NdCl}_3 \cdot 6\text{H}_2\text{O}$ (0.050 mmol) and H_4tpabn (0.10 mmol) in water (9.0 mL) at pH 6.5 (adjusted by the addition of Et_3N). Small crystals suitable for X-ray diffraction studies appeared after three days. The crystals were filtered, washed with water, and dried under vacuum for a few minutes to yield the Nd-containing polymer $\{[\text{Nd}(\text{tpabn})] \cdot 6\text{H}_2\text{O}\}_\infty$ (**12**) as a white crystalline powder (55% yield). Elemental analysis (%) calcd for $\text{C}_{32}\text{H}_{43}\text{N}_6\text{O}_{15}\text{Nd}$: C 42.90, H 4.84, N 9.38; found: C 43.03, H 4.88, N 9.17.

When the synthesis of the Nd-containing polymer was performed in the presence of KOH as the base, the same polymer $\{[\text{Nd}(\text{tpabn})] \cdot 6\text{H}_2\text{O}\}_\infty$ (**12**) was obtained. Elemental analysis (%) calcd for $\text{C}_{32}\text{H}_{43}\text{N}_6\text{O}_{15}\text{Nd}$: C 42.90, H 4.84, N 9.38; found: C 42.63, H 4.71, N 9.21.

The PXRD patterns of the crystalline solids prepared under different basic conditions were consistent with the calculated patterns, thus confirming the identity and phase purity of these polymers. The TGA of **12** displayed a first weight loss of 11.8% between 30 and 110°C, which corresponds to the loss of the six solvated water molecules (calcd: 12.06%). Decomposition of the complex was observed from 250°C (see Figure S3 in the Supporting Information).

The six guest water molecules could be removed by drying the solid under vacuum at 130°C for six days, thus yielding the dehydrated compound $\{[\text{Nd}(\text{tpabn})] \cdot 3\text{H}_2\text{O}\}_\infty$ (**13**). Elemental analysis (%) calcd for $\text{C}_{32}\text{H}_{31}\text{N}_6\text{O}_9\text{Nd}$: C 48.78, H 3.97, N 10.67; found: C 48.50, H 3.96, N 10.47.

Single-crystal X-ray diffraction studies: Because of the weak diffracting power and small size of the crystals, determination of their crystal structures required the use of synchrotron radiation. To avoid the loss of solvent, the crystals were handled in the mother liquid, transferred to the diffraction oil (Hampton research) without exposure to air, and frozen instantly at 100 K. Synchrotron radiation with calibrated wavelengths of

approximately $\lambda = 0.70 \text{ \AA}$, area detectors MAR345 (image plate IP), or KUMA Onyx (CCD) were used for data collection at the Swiss–Norwegian Beam Lines at the ESRF. The structures were solved by direct methods and refined by a full-matrix least-squares technique on F^2 using the SHELX97 program package.^[39a] The experimental details of the X-ray data collection for all the complexes are given in Table 1.^[39b]

Powder X-ray diffraction studies: The PXRD data for isolated solid samples were recorded on a Panalytical X'Pert MPD diffractometer at 40 kV and 40 mA with $\text{CoK}\alpha$ radiation ($\lambda = 1.789 \text{ \AA}$) with a scan speed of $0.05^\circ \text{ min}^{-1}$ and a step size of 0.01° in 2θ . The PXRD data for crystalline samples in their mother liquor were recorded in sealed capillary tubes at the ESRF on a MAR354 image plate detector at a wavelength of $\lambda = 0.711 \text{ \AA}$. The cell parameters of the polymers were determined by automatic indexing by using DicVol04. Only one solution was found, which is closely related to the single-crystal model. The cell parameters were refined by using the Rietveld method.

Spectroscopic measurements: The luminescence measurements were carried out on powder samples inside capillary tubes. Low-resolution luminescence measurements (spectra and lifetimes) were recorded on a Fluorolog FL 3-22 spectrometer from Spex-Jobin-Yvon-Horiba with double-grating emission, excitation monochromators, and a R928P photomultiplier. For measurements in the near-IR (NIR) spectral range, the spectrometer was fitted with a second measuring channel equipped with a FL-1004 single-grating monochromator and light intensity was measured by two Jobin–Yvon solid-state InGaAs detectors: 1) DSS-IGA020L, cooled to 77 K (range: 800–1600 nm) and 2) S-IGA020A (range: 800–1700 nm) working at room temperature and inserted into a LN2 housing including an elliptical mirror (beam path: 90°) and coupled to a Jobin–Yvon SpectraAcq2 data acquisition system. The equipment and experimental procedures for luminescence measurements in the visible and NIR range have been reported previously.^[41] All the spectra were corrected for the instrumental functions. Lifetimes were measured in the time-resolved mode and are averages of three independent measurements, which were made by monitoring the decay at the maxima of the emission spectra. The monoexponential decays were analyzed with Origin 7.0. Quantum yields of the polymers in the solid state and at room temperature were determined by using an absolute method with a home-modified integrating sphere from Oriel and the previously described procedure.^[42] The spectra were corrected for the instrumental function.

Results and Discussion

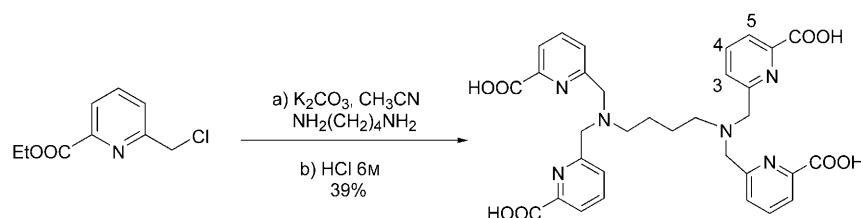
Ligand synthesis: The decadentate ligand N,N,N',N' -tetrakis[(6-carboxypyridin-2-yl)methyl]butylenediamine (H_4tpabn) was readily obtained in five steps from commercially available 2,6-dipicolinic acid and 1,4-diaminobutane dihydrochloride in a global yield of 27% (Scheme 3). Four deprotonation constants ($\text{p}K_{\text{a},1} = 3.2(3)$, $\text{p}K_{\text{a},2} = 3.7(2)$, $\text{p}K_{\text{a},3} = 6.99(4)$, $\text{p}K_{\text{a},4} = 8.08(3)$) were determined for the $[\text{H}_6\text{tpabn}]^{2+}$ ion by potentiometric titration. The two highest $\text{p}K_{\text{a}}$ values were assigned to the aliphatic amine nitrogen atoms.

Synthesis and characterization of the coordination polymers: The 1:1 reaction of $\text{LnCl}_3 \cdot 6\text{H}_2\text{O}$ ($\text{Ln} = \text{Nd, Eu, Tb, Er}$) with the ligand H_4tpabn in water at pH 6–7 leads to the immediate formation of a precipitate that is highly insoluble in water or common organic solvents, thus rendering the preparation of crystals suitable for characterization by X-ray diffraction studies difficult. Conversely, the reaction of $\text{LnCl}_3 \cdot 6\text{H}_2\text{O}$ ($\text{Ln} = \text{Nd, Eu, Tb, Er}$) with the ligand H_4tpabn

Table 1. Crystal data and structure refinements for **2**, **4**, **7**, and **10–12**.^[a]

	2	4	7	10	11	12
formula	{[Er(Htpabn)]·14 H ₂ O} _∞	{[Er(Htpabn)]·5.5 H ₂ O} _∞	{[Eu(Htpabn)]·10 H ₂ O} _∞	{[Tb(Htpabn)]·10 H ₂ O} _∞	{[Tb(Htpabn)]·8 H ₂ O} _∞	{[Nd(tpabn)]H ₃ O·6 H ₂ O} _∞
empirical formula	C ₃₂ H ₅₇ N ₆ O ₂₂ Er	C ₃₂ H ₄₀ N ₆ O _{13.5} Er	C ₃₂ H ₄₉ N ₆ O ₁₈ Eu	C ₃₂ H ₄₉ N ₆ O ₁₈ Tb	C ₃₂ H ₄₅ N ₆ O ₁₆ Tb	C ₃₂ H ₄₃ N ₆ O ₁₅ Nd
<i>M_w</i>	1045.09	891.96	957.74	964.69	3694.48	895.96
<i>T</i> [K]	100	293	100	100	100	100
crystal system	monoclinic	monoclinic	monoclinic	monoclinic	monoclinic	triclinic
space group	<i>P</i> 2 ₁ / <i>n</i>	<i>P</i> 2 ₁ / <i>n</i>	<i>C</i> 2/ <i>c</i>	<i>C</i> 2/ <i>c</i>	<i>P</i> 2 ₁ / <i>n</i>	<i>P</i> $\bar{1}$
<i>a</i> [Å]	16.1573(2)	17.1057(7)	20.3149(2)	20.4044(2)	18.5314(5)	10.7533(10)
<i>b</i> [Å]	14.2632(2)	14.2608(5)	14.3423(1)	14.2459(1)	13.9969(4)	12.7831(11)
<i>c</i> [Å]	18.6231(3)	14.8950(6)	28.1227(2)	27.9874(3)	15.0320(4)	13.8556(16)
α [°]	90	90	90	90	90	81.976(8)
β [°]	94.194(1)	100.431(4)	105.2833(8)	104.754(1)	104.977(3)	78.009(9)
γ [°]	90	90	90	90	90	84.563(7)
<i>V</i> [Å ³]	4280.28(10)	3573.5(2)	7904.11(10)	7867.10(12)	3766.6 (2)	1840.5(3)
<i>Z</i>	4	4	8	8	4	2
ρ [g cm ⁻³]	1.622	1.658	1.611	1.629	1.629	1.617
μ [mm ⁻¹]	2.050	2.423	1.670	1.881	1.957	1.489
instrument	KUMA CCD	MAR345 IP	MAR345 IP	MAR345 IP	KUMA CCD	MAR345 IP
θ [°]	1.81–27.50	2.78–23.50	1.79–27.40	2.70–25.00	3.83–30.00	1.94–22.50
reflections collected	32166	29310	36470	23862	15560	7381
independent reflections	9408, <i>R</i> _{int} = 0.0821	5280, <i>R</i> _{int} = 0.0795	8536, <i>R</i> _{int} = 0.0386	6249, <i>R</i> _{int} = 0.0373	9806, <i>R</i> _{int} = 0.0972	4487, <i>R</i> _{int} = 0.0289
parameters	554	475	521	520	501	544
GOF on <i>F</i> ² _[b]	1.151	1.098	1.035	1.082	0.998	1.046
<i>R</i> ₁ , <i>R</i> ₂	0.0919, 0.2177	0.0741, 0.1775	0.0478, 0.1176	0.0493, 0.1248	0.0828, 0.1559	0.0407, 0.0926
[<i>I</i> > 2σ(<i>I</i>)]						
<i>R</i> ₁ , <i>R</i> ₂ (all data)	0.1039, 0.2270	0.0944, 0.1937	0.0599, 0.1252	0.0557, 0.1294	0.1701, 0.1984	0.0450, 0.0961

[a] See reference [39]. [b] Structure was refined on *F*_o² using all data: $wR_2 = [\sum(w(F_o^2 - F_c^2)^2) / \sum w(F_o^2)^2]^{1/2}$, where $w^{-1} = [\sum(F_o^2) + (aP)^2 + (bP)]$ and $P = [\max(F_o^2, 0) + 2F_c^2] / 3$.

Scheme 3. Synthesis of H₄tpabn and its numbering for NMR spectral assignment.

in water at pH 6–7 in a metal/ligand (M/L) ratio of 0.5:1 leads to a solution. Slow diffusion of an additional 0.5 equivalents of the metal into this solution allowed the desired 1:1 complexes in a crystalline form suitable for single-crystal X-ray diffraction studies to be obtained. PXRD experiments indicated that the same compound was obtained by using direct synthesis and slow diffusion as preparation methods, although the diffraction quality was lower in the first case.

Structure of the [Ln(Htpabn)] polymers: The slow diffusion of a solution of one equivalent of LnCl₃·6H₂O (Ln = Tb, Er) in a EtOH/H₂O solvent mixture into a solution of two equivalents of the H₄tpabn ligand and one equivalent of LnCl₃·6H₂O in water at pH 6.5 (adjusted by the addition of Et₃N) led to the isolation of the analytically pure complexes

[Ln(Htpabn)]·5.5 H₂O (Ln = Tb, Er) in 58–60% yield. X-ray quality crystals were obtained for Tb^{III} and Er^{III} complexes by using a similar procedure. Suitable single crystals were selected in the mother liquor and quickly transferred to paratone oil to avoid undesired solvent loss. The X-ray diffraction

study performed on these crystals revealed the presence of 1D lanthanide coordination polymers with the general formula {[Ln(Htpabn)]·14 H₂O}_∞ (Ln = Tb (**1**); Ln = Er (**2**)). The two polymeric chains are isostructural, and accordingly only the crystal packing of the Er^{III}-coordinated chain is shown in Figure 1. Selected distances are shown in Table 2 and selected angles in Table 3. Slow evaporation of the solution that contained crystals of the Er-containing polymer **2** led to the isolation of a second type of crystal containing a decreased number of guest water molecules. Single-crystal X-ray diffraction studies of these crystals revealed a very similar 1D chain in {[Er(Htpabn)]·5.5 H₂O}_∞ (**4**). The structural differences that arose from the different solvation methods are described later.

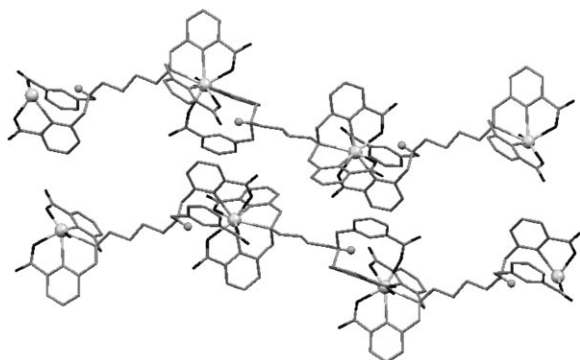


Figure 1. Directional polymeric chains and crystal packing of **2**. Hydrogen atoms that protonate aliphatic nitrogen atoms are shown as spheres. Other hydrogen atoms and water molecules are omitted for clarity.

Table 2. Selected bond lengths [Å] for **1**, **2**, **4**, and **11**.

	M = Tb (1)	M = Er (2)	M = Er (4)	M = Tb (11)
M–O5'	2.290(3)	2.276(7)	2.230(9)	2.298(7)
M–O7'	2.293(3)	2.268(7)	2.249(10)	2.273(7)
M–O1	2.329(3)	2.316(6)	2.296(8)	2.324(7)
M–O3	2.342(3)	2.336(6)	2.293(9)	2.372(7)
M–N3	2.475(3)	2.469(8)	2.441(10)	2.505(8)
M–N2	2.495(3)	2.477(8)	2.494(9)	2.531(8)
M–N1	2.672(3)	2.671(7)	2.710(8)	2.733(8)
M–N5'	2.691(3)	2.679(8)	2.759(10)	2.692(9)
M–N6	3.796(3)	3.801(7)	3.545(9)	3.806(9)
M–N4	4.206(3)	4.234(7)	4.185(9)	4.321(9)

Table 3. Selected angles [°] for **1**, **2**, **4**, and **11**.

	M = Tb (1)	M = Er (2)	M = Er (4)	M = Tb (11)
O5'–M–O7'	81.9(1)	81.8(3)	83.2(4)	83.1(2)
O5'–M–O1	114.8(1)	116.5(3)	111.8(3)	107.0(3)
O7'–M–O1	149.0(1)	147.7(2)	152.0(3)	150.0(2)
O5'–M–O3	145.9(1)	145.2(2)	144.8(4)	146.8(2)
O7'–M–O3	77.6(1)	77.1(2)	79.8(3)	79.4(2)
O1–M–O3	74.6(1)	73.4(2)	74.6(3)	77.2(2)
O5'–M–N3	136.7(1)	136.5(2)	139.5(3)	138.3(3)
O7'–M–N3	81.2(1)	81.9(3)	80.3(4)	78.8(2)
O1–M–N3	99.5(1)	98.1(2)	99.6(3)	107.3(3)
O3–M–N3	66.3(1)	67.1(2)	66.9(3)	64.8(2)
O5'–M–N2	79.7(1)	79.4(3)	77.0(3)	74.9(2)
O7'–M–N2	145.7(1)	145.8(2)	142.6(3)	143.4(2)
O1–M–N2	65.2(1)	66.4(2)	65.4(3)	66.0(3)
O3–M–N2	130.6(1)	131.5(2)	132.3(3)	132.9(2)
N3–M–N2	92.7(1)	92.1(2)	94.6(3)	98.6(3)
O5'–M–N1	73.7(1)	72.7(2)	76.2(3)	76.3(2)
O7'–M–N1	84.3(1)	84.2(2)	82.1(3)	84.1(2)
O1–M–N1	124.4(1)	125.4(2)	123.6(3)	125.5(2)
O3–M–N1	130.1(1)	131.1(2)	130.8(3)	129.0(2)
N3–M–N1	65.2(1)	65.7(2)	65.1(3)	64.8(3)
N2–M–N1	62.8(1)	63.0(2)	62.7(3)	62.7(2)
O5'–M–N5'	64.49(9)	64.9(2)	63.1(3)	65.0(2)
O7'–M–N5'	88.7(1)	88.8(2)	97.4(3)	86.4(2)
O1–M–N5'	77.04(9)	77.2(2)	71.1(3)	73.5(2)
O3–M–N5'	87.88(9)	87.1(2)	88.8(3)	85.8(2)
N3–M–N5'	153.70(10)	154.0(2)	155.7(3)	148.9(3)
N2–M–N5'	108.73(10)	108.4(2)	101.3(3)	109.3(2)
N1–M–N5'	138.17(9)	137.6(2)	138.9(3)	140.9(2)

Notably, under the chosen synthetic conditions the ligand remains monoprotonated (i.e., Htpabn³⁻) in the terbium and erbium complexes as a result of the high p*K*_a values of the amine nitrogen atoms. Even in the presence of the lanthanide ion, deprotonation of the amine nitrogen atom does not occur and only eight-coordinate complexes are obtained in the presence of erbium and terbium. Attempts were made to isolate a Tb^{III} complex that contained a completely deprotonated ligand by performing the synthesis at a higher pH value (pH 9) to favor the complete deprotonation of the H₄tpabn ligand. However, elemental analysis of the isolated product suggested the presence of a mixture of protonated and deprotonated complexes.

PXRD patterns were measured on bulk crystalline powders from the large-scale synthesis of the terbium complex suspended in their mother liquor. The cell parameters for the {[Tb(Htpabn)]·*x*H₂O}_∞ complex suspended in the mother liquor are *a* = 18.535(4), *b* = 14.083(3), *c* = 15.167(3) Å; α = 90, β = 105.70(2), γ = 90°; *V* = 3811.3(15) Å³. These cell parameters are in agreement with the presence of the octahydrated 1D coordination polymer {[Tb(Htpabn)]·8H₂O}_∞. These results indicated that the number of lattice water molecules can vary even in solution with water depending on the concentration and/or crystal size. The PXRD patterns measured for the powders obtained from the filtration of crystals of the erbium- and terbium-containing polymers also show phase purity (Figure 2). The

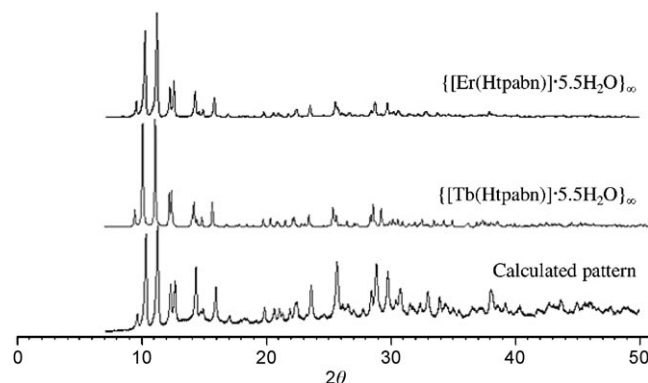


Figure 2. PXRD patterns for the isolated complexes {[Ln(Htpabn)]·5.5H₂O}_∞ (Ln = Tb, Er).

refinement of the cell parameters indicated the presence of the {[Ln(Htpabn)]·5.5H₂O}_∞ complexes, in agreement with the formula obtained from elemental analysis ([{Ln(Htpabn)]·5.5H₂O}_∞ (Ln = Tb and Er). Both X-ray diffraction experiments (single crystal and powder) show that the Tb^{III}- and Er^{III}-based polymers contain a large amount of lattice water molecules that are readily lost by simply removing the polymer from the mother liquor. The removal of water results in a significant modification of the cell parameters.

The single-crystal X-ray structure of **1** and **2** shows the presence of the monoprotonated Htpabn³⁻ ligand, which

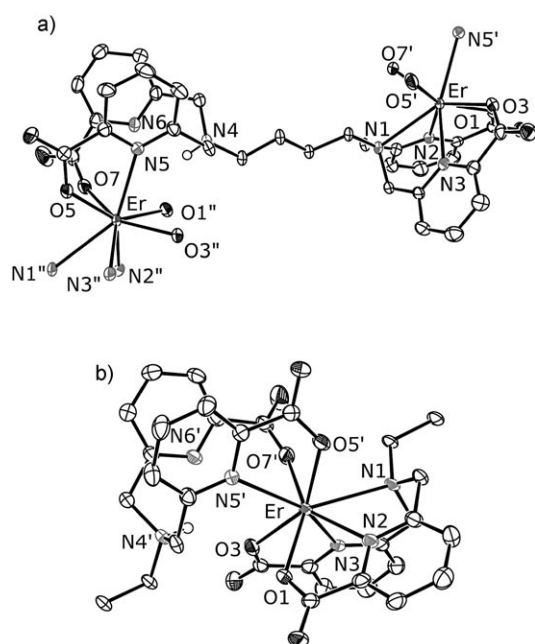


Figure 3. Ortep views of **2**. a) Ligand-coordination mode and b) coordination environment of the lanthanide ion. The ellipsoids are shown at the 50% probability level.

acts as an octadentate ligand that binds two symmetry-related (by the n glide plane) lanthanide ions (Figure 3a), thus leading to the formation of 1D zigzag chains that run along the $(a+c)/2$ diagonal of the unit cell.

The structures of **1** and **2** consist of eight-coordinate lanthanide ions with a distorted bicapped trigonal-prism geometry. The metal atom is coordinated by two carboxylate oxygen atoms, two pyridine (pyr) nitrogen atoms, and one aliphatic nitrogen atom from one ligand molecule and two carboxylate oxygen atoms and one pyridine nitrogen atom from another ligand molecule (Figure 3b). The difference between the mean Ln–donor atom bond lengths (0.001–0.014 Å) in **1** and **2** is significantly smaller than the difference between the ionic radii of Tb and Er for the coordination number eight (0.036 Å). This aspect suggests that the ligand does not adapt very well to lanthanide ions with different ionic radii. One pyridine nitrogen atom and the protonated aliphatic (aliph) nitrogen atom remain non-coordinated with $\text{Ln}\cdots\text{N}_{\text{pyr}}=3.8$ Å and $\text{Ln}\cdots\text{N}_{\text{aliph}}=4.2$ Å for both ions. Water molecules do not coordinate the metal atom. The protonation of one aliphatic nitrogen (N4) atom breaks the ligand symmetry, thus yielding two different coordination sites. This process results in the formation of a directional chain. However, the centrosymmetric packing of the 1D chains in the crystalline phase results in a nonpolar solid (Figure 1). The stacking interactions of $\text{C}-\text{H}\cdots\pi$ and $\pi\cdots\pi$ between the pyridine rings connect the 1D coordination polymers to yield a 3D network. The water molecules located between 1D chains form an extended network of hydrogen bonds between themselves and with the carboxylate oxygen atoms of different chains. The shortest distance be-

tween the lanthanide ions in the polymeric chain is 12.27 and 12.19 Å for Er and Tb, respectively, with an angle Ln–Ln–Ln of 150.1 and 149.4° for Er and Tb, respectively. The shortest Ln \cdots Ln interchain distance is 8.18 and 8.13 Å for Er and Tb, respectively.

These results show that the proposed topological approach that uses a flexible high-denticity linker is efficient in promoting the supramolecular assembly of 1D polymers, even when the denticity does not perfectly match the lanthanide requirements.

However, attempts to obtain single crystals of the europium-containing 1D polymer with the Htpabn^{3-} ion by using the procedure used for polymers **1** and **2** failed to give crystals suitable for X-ray diffraction studies. Indexing of the PXRD pattern yielded five possible solutions in the space group $P2_1/n$ but none corresponded to the isolated crystallographic structures. Crystals suitable for X-ray diffraction studies were obtained by diffusion of one equivalent of $\text{EuCl}_3\cdot 6\text{H}_2\text{O}$ into a 2:1 ligand/metal solution with KOH instead of Et_3N as the base. Single-crystal X-ray diffraction studies revealed the presence of a nine-coordinate europium center included in a 2D coordination polymer $\{[\text{Eu}(\text{Htpabn})]\cdot 10\text{H}_2\text{O}\}_\infty$ (**7**; Figure 4). By using the same proce-

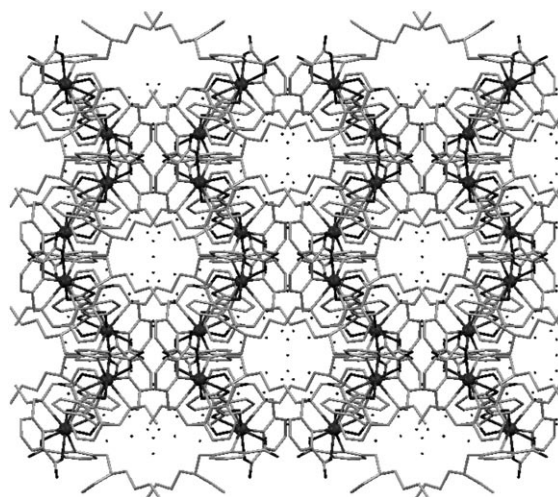


Figure 4. Diagram of the 2D network formed by **7** and **10** (view along the c axis). Hydrogen atoms and water molecules are omitted for clarity.

cedure, $\{[\text{Eu}(\text{Htpabn})]\cdot 8.5\text{H}_2\text{O}\}_\infty$ (**8**) was isolated in 66% yield after filtration of the final product. PXRD studies on the crystalline sample suspended in the mother liquor confirmed the presence of only one phase that corresponded to the 2D network $\{[\text{Eu}(\text{Htpabn})]\cdot 10\text{H}_2\text{O}\}_\infty$ (**7**; see Figure S4 in the Supporting Information).

We also prepared the terbium-containing polymer with KOH as the base to investigate the potential effect of the base on the formation of the 1D and 2D polymeric phases. Two different types of single crystals were isolated from this reaction that correspond to two different polymorphic forms: a 2D polymeric network $\{[\text{Tb}(\text{Htpabn})]\cdot 10\text{H}_2\text{O}\}_\infty$

(**10**) and a 1D polymer $\{[\text{Tb}(\text{Htpabn})] \cdot 8\text{H}_2\text{O}\}_\infty$ (**11**). However, PXRD studies carried out on the isolated powder obtained from a large-scale synthesis with KOH shows only the presence of the 1D network $\{[\text{Tb}(\text{Htpabn})] \cdot 5.5\text{H}_2\text{O}\}_\infty$ (see Figure S5 in the Supporting Information). Similarly, the PXRD studies carried out on the erbium-containing polymers prepared with KOH shows only the presence of the 1D network $\{[\text{Er}(\text{Htpabn})] \cdot 5.5\text{H}_2\text{O}\}_\infty$ (**4**). This result confirms that the type of base used in the synthesis of the lanthanide complexes plays a role only for ions with intermediate ionic radii, for which nine- and eight-coordinate structures have similar stabilities.

The single-crystal X-ray structure of the 2D coordination Eu^{III} - and Tb^{III} -containing polymers **7** and **10** shows the presence of the monoprotonated Htpabn^{3-} ion, which acts as a nonadentate ligand that binds three lanthanide ions related by the symmetry axes 2 into a 2D network (Figure 5).

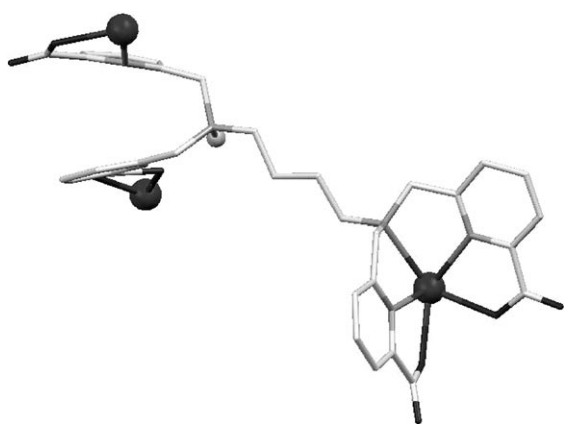


Figure 5. Mercury diagram showing the coordination mode of the Htpabn^{3-} ligand in **7** and **10**.

The structure contains nine-coordinate lanthanide ions with irregular coordination geometries. Each metal atom binds two pyridine nitrogen atoms, one amine nitrogen atom, and two carboxylate oxygen atoms from one ligand; one pyridine nitrogen atom and one carboxylate oxygen atom from one picolinate unit of an adjacent ligand; and two carboxylate oxygen atoms from a picolinate unit of another adjacent ligand (Figure 6). Water molecules do not coordinate the metal atom but form an extended network of hydrogen bonds. The water molecules are located in channels $8 \times 6 \text{ \AA}^2$ in width. Selected angles and distances for complexes **7** and **10** are shown in Tables 4 and 5, respectively. In both 2D networks, the shortest $\text{Ln} \cdots \text{Ln}$ distance is 10.40 \AA .

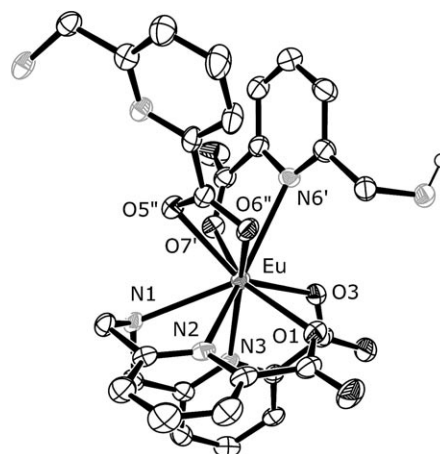


Figure 6. Ortep view of $\{[\text{Eu}(\text{Htpabn})] \cdot 10\text{H}_2\text{O}\}_\infty$ (**7**). Ellipsoids are shown at the 50% probability level.

The ligand remains monoprotonated in complexes **7** and **10**. Attempts to isolate the deprotonated europium complex at higher pH values only resulted in mixtures of protonated and unprotonated complexes. The presence of a protonated nitrogen atom in the ethylenediamine spacer significantly decreases the preorganization of the multidentate linker. Notably, when the aliphatic nitrogen atom of the diamine spacer is protonated, the directing effect of the linker is lost at least on one side. The two picolinate units bound to the protonated amine nitrogen atom are no longer connected into a pentadentate ligand, and therefore the decreased chelate effect is not sufficient to favor the coordination of only one metal ion (1D polymer) relative to two different lanthanide ions (2D polymer). In the absence of sufficient ligand preorganization, the favored coordination number of the metal becomes the discriminating factor between possible isomeric structures. As a result, the formation of 1D coordination polymers is favored with small lanthanide ions inde-

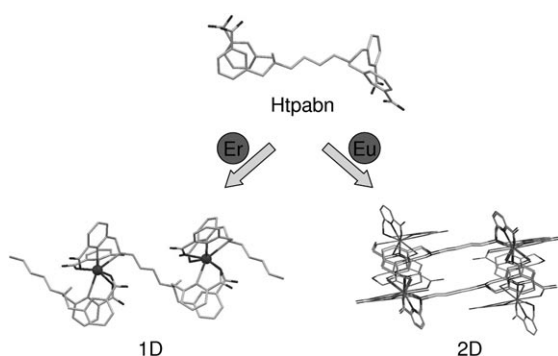
Table 4. Selected angles [°] for **7** and **10**.

	M = Eu (7)	M = Tb (10)		M = Eu (7)	M = Tb (10)
O7'-M-N6'	64.82(12)	65.28(15)	O5''-M-N3	135.71 (12)	136.22 (15)
O1-M-N6'	99.73(13)	98.91(16)	O6''-M-N3	154.74(12)	154.43(14)
O3-M-N6'	76.17(12)	74.85(15)	O7'-M-O1	148.83(13)	148.36(16)
O5-M-N6'	71.81(12)	72.08(16)	O7'-M-O3	78.40(12)	77.91(15)
O6''-M-N6'	68.70(11)	68.88(15)	O7'-M-O5''	77.70(11)	77.94(14)
O7'-M-N1	82.30(12)	81.92(15)	O7'-M-O6''	118.88(11)	119.56(14)
O1-M-N1	122.12(12)	122.80(15)	O5''-M-O1	125.06(12)	125.09(15)
O3-M-N1	126.42(12)	126.99(16)	O5''-M-O3	145.92(12)	144.92(14)
O5''-M-N1	73.53(12)	73.70(16)	O5''-M-O6''	51.11(10)	51.51(14)
O6''-M-N1	107.77(11)	108.22(15)	O3-M-O1	71.44(12)	71.33(15)
O7'-M-N2	143.88(13)	143.64(16)	O3-M-O6''	125.37(11)	124.42(15)
O1-M-N2	65.42(13)	66.24(16)	O1-M-O6''	74.82(12)	74.35(15)
O3-M-N2	127.12(13)	128.57(15)	N2-M-N3	85.23(12)	85.98(16)
O5''-M-N2	85.74(12)	85.05(15)	N2-M-N6'	138.88(12)	138.32(17)
O6''-M-N2	70.37(12)	69.60(16)	N2-M-N1	62.17(12)	62.42(16)
O7'-M-N3	84.71(12)	84.58(15)	N3-M-N6'	134.63(12)	134.33(16)
O1-M-N3	89.40(12)	89.24(15)	N3-M-N1	63.95(12)	64.22(16)
O3-M-N3	64.85(12)	65.45(15)	N6'-M-N1	136.16(12)	136.45(15)

Table 5. Selected bond lengths [\AA] for **7** and **10**.

	M = Eu (7)	M = Tb (10)
M–O7'	2.345(3)	2.314(4)
M–O1	2.379(4)	2.360(4)
M–O3	2.388(3)	2.374(4)
M–O5''	2.505(3)	2.492(4)
M–O6''	2.609(4)	2.572(5)
M–N2	2.507(4)	2.483(5)
M–N3	2.541(4)	2.508(5)
M–N6'	2.676(4)	2.647(5)
M–N1	2.715(4)	2.702(5)

pendent of the basic conditions used, whereas the nine-coordinate 2D network is clearly favored with europium (which favors a larger coordination number) and can be obtained in a pure form by an appropriate choice of base (Scheme 4).



Scheme 4. The formation of 1D and 2D networks for the Er and Eu ions, respectively.

For ions of intermediate size, such as terbium, the formation of the polymorphic 2D isomer is possible.

For the terbium ion, the formation of eight-coordinate 1D chains is favored but the 2D isomer can also form as a minor product under favorable conditions (i.e., base and concentration). These results show that the flexible multidentate ligand Htpabn^{3-} ion can lead to the formation of supramolecular isomers for lanthanide ions for which the eight- and nine-coordinate geometries have similar stabilities. It seems that the nature of the base can influence the final geometry, with KOH favoring the 2D arrangement. A possible explanation of the effect of the base in favoring one isomer could be the presence of potassium-coordinated intermediates.^[29]

Structure of the $[\text{Nd}(\text{tpabn})]^-$ polymer: The residual proton on the Htpabn^{3-} ligand significantly decreases the preorganization of the multidentate linker, which leads to polymorphism in some cases and therefore does not allow validation of the topological approach to the preparation of 1D polymers. However, in the case of the neodymium ion full ligand deprotonation occurs and the effect of the preorganization of the multidentate linker becomes evident. The reaction of $\text{NdCl}_3 \cdot 6\text{H}_2\text{O}$ with the H_4tpabn ligand (the pH value

was adjusted by the addition of Et_3N or KOH) led to the isolation of the analytically pure complex $[\text{Nd}(\text{tpabn})]\text{H}_3\text{O} \cdot 6\text{H}_2\text{O}_\infty$ (**12**) in 55% yield. The X-ray diffraction study revealed the presence of a 1D lanthanide-coordination polymer with a zigzag structure and a general formula of $[\text{Nd}(\text{tpabn})]\text{H}_3\text{O} \cdot 6\text{H}_2\text{O}_\infty$ (**12**; Figure 7). Selected

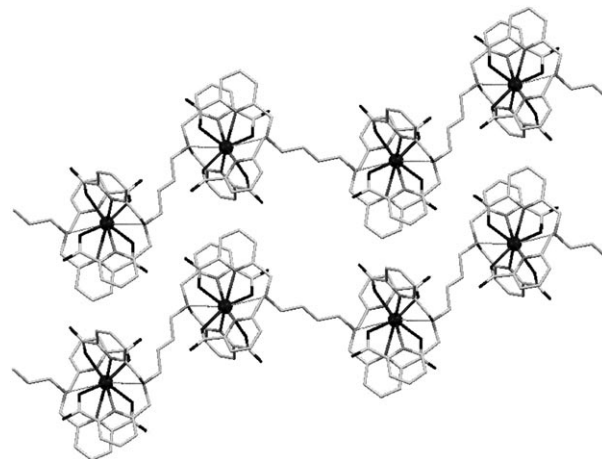


Figure 7. Zigzag chain structure and crystal packing of **12**. Hydrogen atoms and water molecules are omitted for clarity.

angles and bond distances are presented in Table 6. The PXRD studies were carried out on crystalline samples obtained in the presence of different bases (KOH or Et_3N) and suspended in the mother liquor (Figure 8). The PXRD

Table 6. Selected bond lengths [\AA] and angles [$^\circ$] for **12**.

Nd–O7'	2.495(4)	O1–Nd–N4'	70.21(12)
Nd–O1	2.491(4)	O3–Nd–N4'	72.88(13)
Nd–O3	2.411(4)	O5'–Nd–N4'	117.90(13)
Nd–O5'	2.430(4)	O7'–Nd–N1	62.84(13)
Nd–N5'	2.708(5)	O1–Nd–N1	108.03(13)
Nd–N2	2.699(5)	O3–Nd–N1	122.13(13)
Nd–N3	2.701(5)	O5'–Nd–N1	72.26(12)
Nd–N6'	2.675(5)	O3–Nd–O5'	81.98(14)
Nd–N4'	2.969(5)	O3–Nd–O1	71.33(13)
Nd–N1	3.056(5)	O5'–Nd–O1	148.54(13)
O7'–Nd–N6'	60.67(13)	O3–Nd–O7'	158.17(13)
O1–Nd–N6'	78.99(13)	O5'–Nd–O7'	79.50(13)
O3–Nd–N6'	127.93(14)	O1–Nd–O7'	129.57(13)
O5'–Nd–N6'	131.87(13)	N2–Nd–N3	85.73(14)
O7'–Nd–N2	76.41(14)	N2–Nd–N6'	69.95(14)
O1–Nd–N2	61.34(14)	N2–Nd–N4'	112.75(14)
O3–Nd–N2	124.67(14)	N2–Nd–N5'	149.60(15)
O5'–Nd–N2	128.06(14)	N2–Nd–N1	55.81(14)
O7'–Nd–N3	119.82(14)	N2–Nd–N5'	149.60(15)
O1–Nd–N3	84.80(13)	N2–Nd–N1	55.81(14)
O3–Nd–N3	62.20(14)	N3–Nd–N6'	155.10(14)
O5'–Nd–N3	67.82(13)	N3–Nd–N4'	133.69(14)
O3–Nd–N3	62.20(14)	N3–Nd–N5'	121.84(14)
O5'–Nd–N3	67.82(13)	N3–Nd–N1	60.18(13)
O7'–Nd–N5'	78.33(13)	N4'–Nd–N5'	59.09(13)
O1–Nd–N5'	127.93(13)	N4'–Nd–N6'	56.96(13)
O3–Nd–N5'	82.86(14)	N4'–Nd–N1	164.14(13)
O5'–Nd–N5'	62.14(14)	N5'–Nd–N6'	83.05(14)
O7'–Nd–N4'	105.99(13)	N5'–Nd–N1	123.96(14)

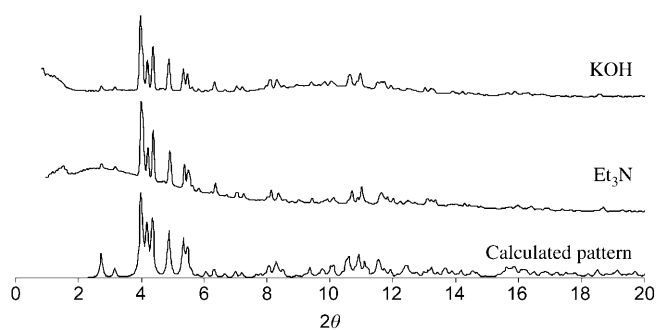


Figure 8. PXRD pattern of the $[\text{Nd}(\text{tpabn})]\text{H}_3\text{O}\cdot 8.5\text{H}_2\text{O}$ complex (suspended in the mother liquor) synthesized with KOH (top) and Et_3N (middle) as the bases. The calculated pattern that used a single-crystal model of **12** and Rietveld-refined cell parameters is given (bottom).

data of the suspended $\{[\text{Nd}(\text{tpabn})]\text{H}_3\text{O}\cdot n\text{H}_2\text{O}\}_\infty$ polymer were indexed in the triclinic space group with the cell parameters close to the single-crystal structure of $\{[\text{Nd}(\text{tpabn})]\text{H}_3\text{O}\cdot 6\text{H}_2\text{O}\}_\infty$ (**12**). The refined data (i.e., $a = 10.595(3)$, $b = 13.028(5)$, $c = 15.683(5)$ Å; $\alpha = 83.11(2)$, $\beta = 72.92(2)$, $\gamma = 83.23(2)^\circ$; $V = 2046.5(12)$ Å³) suggest that the 1D polymer suspended in the solution contains more water molecules of crystallization, and its composition estimated from the cell volume is $\{[\text{Nd}(\text{tpabn})]\text{H}_3\text{O}\cdot 8.5\text{H}_2\text{O}\}_\infty$. The single-crystal X-ray structure of **12** shows the presence of a fully deprotonated tpabn^{4-} ligand, which acts as a decaden-tate ligand and binds two neodymium ions related by the inversion center (Figure 7). This outcome leads to the formation of a 1D zigzag chain that runs along the $(b+c)$ direction of the unit cell. The structure contains ten-coordinate neodymium ions with a slightly distorted bicapped square antiprismatic geometry (Figure 9). The neodymium atom is coordinated by four carboxylate oxygen atoms, four pyridine nitrogen atoms, and two aliphatic nitrogen atoms. The Nd–O and Nd–N_{pyr} lengths are in the range of reported values, whereas longer lengths were found for the aliphatic amine nitrogen atoms (2.969(5) and 3.056(5) Å for Nd–N4 and Nd–N1, respectively). Similar Ln–N lengths were observed

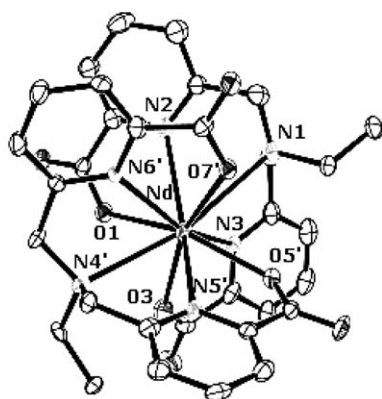


Figure 9. Ortep view of the coordination environment of the Nd center in $\{[\text{Nd}(\text{tpabn})]\text{H}_3\text{O}\cdot 6\text{H}_2\text{O}\}_\infty$ (**12**). Ellipsoids are shown at the 50% probability level.

in the ten-coordinate mononuclear $[\text{Ln}(\text{tpaen})]\text{K}$ complexes (mean $\text{M}-\text{N}_{\text{amine}}$: 2.91(1) and 2.91(4) Å for Eu and Ce, respectively).^[29]

Water molecules do not coordinate the metal atoms, but are only present as guest molecules. Instead of the expected Et_3NH^+ counterion, a protonated water molecule located between the 1D chains provides the required charge balance, thus resulting in strong hydrogen bonds between Ow4 and Ow7. A network of hydrogen bonds connects the lattice water molecules to the carboxylate groups of the 1D chains to yield a 3D network. The stacking interactions $\text{C}-\text{H}\cdots\pi$ and $\pi\cdots\pi$ are also observed between the pyridine rings of different chains. The shortest distance between the lanthanide ions in the polymeric chain is 9.57 Å, whereas the shortest distance between neodymium ions in two different chains is 10.75 Å. The flexible spacer makes the chain undulated, with an angle Nd–Nd–Nd of 143.2°. A comparison of the structural parameters of the neodymium and erbium complexes **12** and **4**, which contain a similar number of guest water molecules, shows that the difference in coordination number and overall charge does not lead to dramatic structural changes. The two 1D chains show very similar intermetallic distances, whereas the Ln–Ln–Ln angle is smaller for the Nd complex (143°) than the angles for the Tb and Er (149–150°).

The TGA of the complex $\{[\text{Nd}(\text{tpabn})]\text{H}_3\text{O}\cdot 6\text{H}_2\text{O}\}_\infty$ showed that six guest water molecules can be removed between 30 and 110 °C (weight loss: 11.8%, calculated: 12.06%). The decomposition of the complex started above 250 °C. The hydrated Nd complex does not display a detectable luminescence in the NIR region, but the dehydrated polymer is luminescent. This behavior suggests the absence of disruption of the network after removal of all the guest water molecules.

Despite the high $\text{p}K_{\text{a}}$ value of the Htpabn^{3-} ion, deprotonation of the ligands occurs in the presence of the neodymium ion, which favors high coordination numbers because of its large size, therefore competing more effectively with the proton in binding to the nitrogen atom. Although high coordination numbers can be observed for the smaller lanthanide ions in the presence of suitably designed predisposed^[45] or preorganized multidentate ligands, their preferred coordination number is usually lower than the one of early lanthanides in the absence of a strong chelate effect. The change in coordination number with a given set of ligands usually occurs at the gadolinium ion.

It should be noted that the full deprotonation of the spacer leads to the formation of the anticipated 1D polymer as the only product in the presence of the nine-coordinate neodymium ions. The higher preorganization of the deprotonated linker tpabn^{4-} ion with respect to the protonated linker Htpabn^{3-} ion allows the preparation of the desired 1D coordination polymer, even in the presence of a large ion. Conversely, the 2D coordination polymers are favored for nine-coordinate lanthanides in the presence of the Htpabn^{3-} ion. These results show that a rational approach to the synthesis of lanthanide-coordination polymers is pos-

sible by using appropriate ligand design. Future work will be directed to extend this approach to the design of networks of higher dimensionality.

Stability of the polymers to the removal of the molecules of water of crystallization:

The stability of the $[\text{Ln}(\text{Htpabn})]$ frameworks and their ability to undergo reversible structural transformations were investigated by TGA and PXRD. In the 2D Eu framework $\{[\text{Eu}(\text{Htpabn})]\cdot 10\text{H}_2\text{O}\}_\infty$ (**7**), the guest water molecules can be partially removed by drying the crystals under vacuum at 130°C for 6 days, thus yielding $\{[\text{Eu}(\text{Htpabn})]\cdot 5\text{H}_2\text{O}\}_\infty$ (**9**). The PXRD data of the resulting partially dehydrated complex (shown in Figure 10) could not

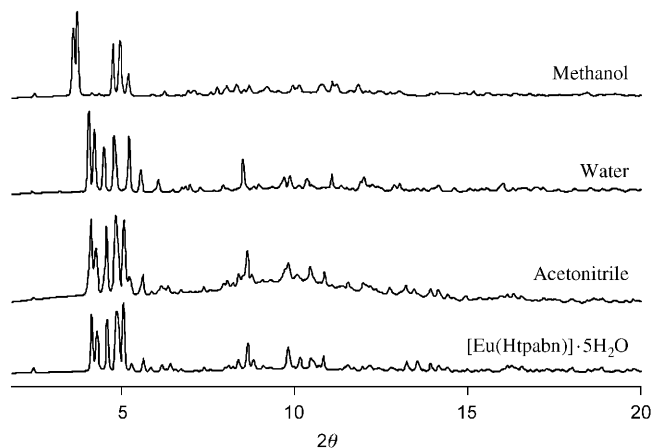


Figure 10. PXRD studies of the absorption of solvent molecules in the $\{[\text{Eu}(\text{Htpabn})]\cdot 5\text{H}_2\text{O}\}_\infty$ (**9**) complex.

be fit by using the crystal data of the hydrated complex **7** probably because of the important effect of water removal on the structure. Complete removal of the guest water molecules from the 2D europium-containing polymer was impossible, and the use of high temperatures resulted in the polymer decomposition. These results are in agreement with the TGA performed on the isolated complex $\{[\text{Eu}(\text{Htpabn})]\cdot 8.5\text{H}_2\text{O}\}_\infty$ (**8**), which showed the loss of 6.50%, which corresponds to only 3.5 water molecules (calcd: 6.77%), between 30 and 110°C . The decomposition of the complex started above 250°C .

The absorption of different guest molecules by the $\{[\text{Eu}(\text{Htpabn})]\cdot 5\text{H}_2\text{O}\}_\infty$ complex was investigated by PXRD studies. The crystalline phase of the $\{[\text{Eu}(\text{Htpabn})]\cdot 5\text{H}_2\text{O}\}_\infty$ complex did not change when exposed to acetonitrile and only changed slightly after absorption of water (Figure 10). However, a new crystalline phase formed after absorption of methanol (Figure 10). We were unable to assign the new structure on the basis of the previously isolated crystal forms.

These results indicate that the removal of solvate water molecules is not reversible for the 2D europium-containing polymer. This behavior is probably because of a significant irreversible modification of the crystal structure. Conversely, the new structure can selectively absorb methanol, which leads to significant structural changes. Luminescence mea-

surements were performed on the europium complex before and after the absorption of methanol to study the influence of this solvent on the luminescence properties of the complex. A significant decrease in the luminescence lifetime and quantum yield is associated with the absorption of methanol and with the formation of the new structural phase (see below).

The TGA of the 1D polymers **1** and **2** showed that all the solvate water molecules can be removed from **1** and **2** ($\{[\text{Ln}(\text{Htpabn})]\cdot 14\text{H}_2\text{O}\}_\infty$) between 30 and 110°C without decomposition of the complex, which only started above 250°C . As mentioned in the previous section, isolation of complexes **1** and **2** by filtration results in the partial loss of guest water molecules with respect to the single crystals, which were directly analyzed in the mother liquor and afforded the $[\text{Ln}(\text{Htpabn})]\cdot 5.5\text{H}_2\text{O}$ complexes. These complexes were heated at 130°C under reduced pressure for six days. Elemental analyses performed in an argon atmosphere on the resulting compound were in agreement with the removal of all the water molecules. The luminescence quantum yield measured on the isolated $\{[\text{Tb}(\text{Htpabn})]\cdot 5.5\text{H}_2\text{O}\}_\infty$ complex remained unchanged after removal of all the solvate water molecules, thus indicating the absence of a significant structural modification of the network. The PXRD patterns confirmed that the 1D chain is flexible and does not collapse when some or all the solvate water molecules are removed (Figure 11). The process of water reabsorption into the an-

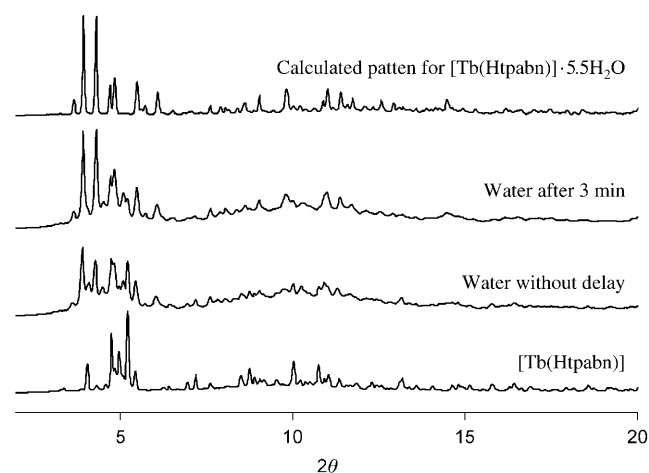


Figure 11. PXRD studies of the absorption of water in the anhydrous $[\text{Tb}(\text{Htpabn})]$ (**5**) complex and the calculated pattern of $\{[\text{Tb}(\text{Htpabn})]\cdot 5.5\text{H}_2\text{O}\}_\infty$.

hydrous compounds was followed by PXRD. These studies showed that the anhydrous Tb^{III} complex can reversibly reabsorb some water molecules to yield the $\{[\text{Tb}(\text{Htpabn})]\cdot 5.5\text{H}_2\text{O}\}_\infty$ complex (Figure 11), thus regaining the original structure. Furthermore, the complete suspension of the $\{[\text{Tb}(\text{Htpabn})]\cdot 5.5\text{H}_2\text{O}\}_\infty$ complex in water yielded a PXRD pattern identical to that of $\{[\text{Tb}(\text{Htpabn})]\cdot 8\text{H}_2\text{O}\}_\infty$ (**11**), which confirms that the removal and absorption of water molecules can be reversible (Figure 12).

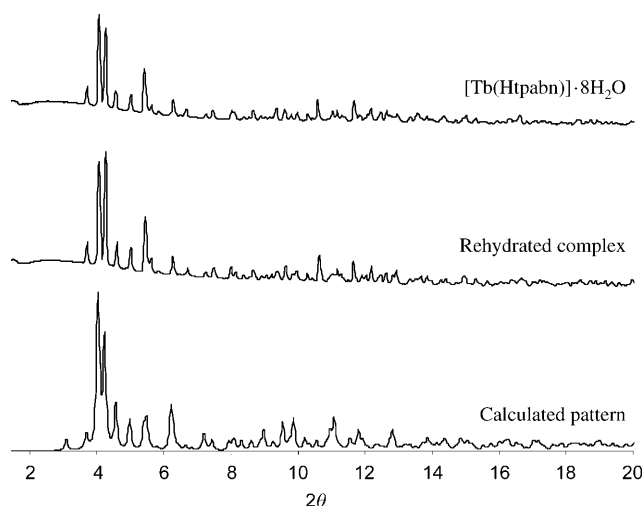


Figure 12. PXRD patterns of the hydration of 1D polymer $\{[Ln(Htpabn)]\cdot 5.5H_2O\}_\infty$ (suspended in water) into the 1D polymer $\{[Tb(Htpabn)]\cdot 8H_2O\}_\infty$.

These results indicate that polymers **1** and **2** present a dynamic behavior with a solvent-induced reversible structural transition. A comparative analysis of the structures of the crystals of the terbium and erbium complexes containing a different number of solvating water molecules ($\{[Ln(Htpabn)]\cdot 14H_2O\}_\infty$ ($Ln = Tb$ (**1**), Er (**2**)), $\{[Er(Htpabn)]\cdot 5.5H_2O\}_\infty$ (**4**), and $Tb(Htpabn)\cdot 8H_2O$ (**11**)) allowed clear assessment of the structural effects of guest mol-

ecules on the 3D packing of these zigzag chains (Figure 13). The structure of the coordination polymer **2** is very similar to polymer **4**. The main differences between the structures of **2** and **4** are highlighted in Figure 13. Although the angle $Er-Er-Er$ remains unchanged, the distances between two metal ions within the chain are significantly shorter in **4** than in **2** (10.63 and 12.27 Å, respectively).

Because of a cooperative effect, the inclusion of additional water molecules in the network results in additional hydrogen bonding between the guest water molecules, which are also hydrogen bound to the carboxylate oxygen atoms of the chains. The flexible aliphatic chains unfold to accommodate additional water molecules between the chains without disruption of the 3D network that results from inter-chain $C-H\cdots\pi$ and $\pi\cdots\pi$ interactions and hydrogen-bonding interactions of the guest water molecules with the carboxylate chains (Figure 14).

The X-ray analyses of **2** and **4** (representing different hydration states) indicate that the observed dynamism is based on the reversible shrinking and expanding of the chains supported by the flexibility of the butylamine spacer in the multidentate $Htpabn^{3-}$ linker. Although dynamic porous coordination frameworks that show elastic guest accommodation based on hydrogen-bonding interactions are very attractive for the design of highly selective functional materials, they have received less attention than rigid 3D porous materials.^[46] Notably only few examples of dynamic behavior have been previously reported for 1D chains,^[34,47,48] and compounds **2** and **4** are to our knowledge the first that involve lanthanide ions.

Furthermore, the reversible solvent inclusion of water molecules is also associated in the case of erbium and neodymium to significant differences in the luminescence efficiency as a result of the important deactivation of the NIR emission by the O–H oscillators.

Preliminary absorption studies of other solvent molecules carried out for the anhydrous complex $[Tb(Htpabn)]$ show that neither methanol nor acetonitrile are absorbed, but the absorption process seems to be selective for water. Further studies will investigate other possible guests and their influence on the luminescent properties.

Photophysical studies: Although luminescent lanthanide-based coordination polymers offer great opportunities for the development of probes and sen-

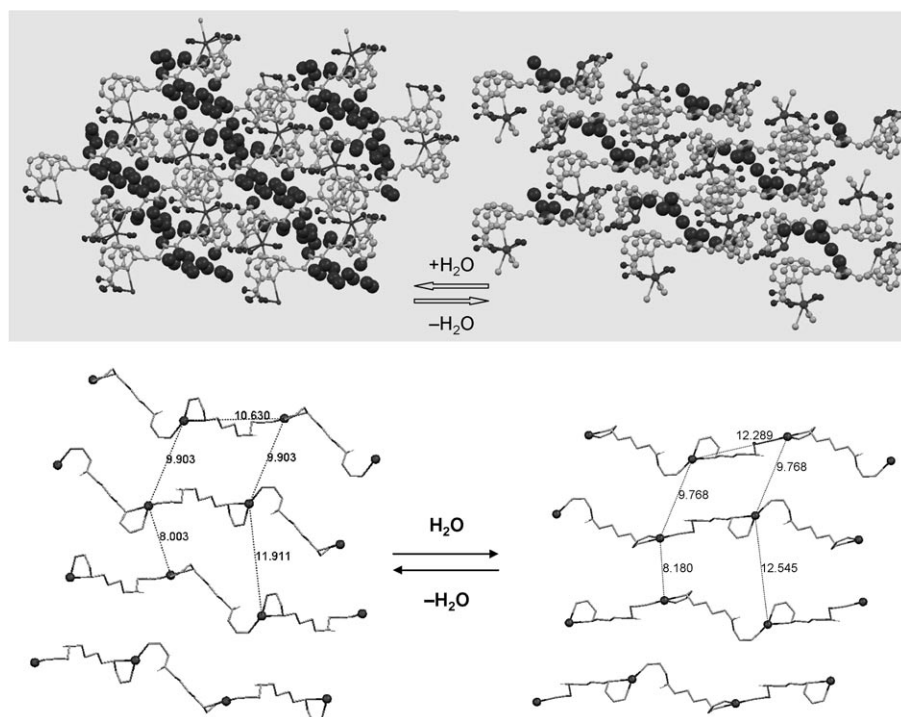


Figure 13. Top: Reversible effect of the increase of guest water molecules (dark gray spheres) on the crystal packing of the $[Er(Htpabn)]$ polymer (left: $\{[Er(Htpabn)]\cdot 14H_2O\}_\infty$ (**2**); right: $\{[Er(Htpabn)]\cdot 5.5H_2O\}_\infty$ (**4**)). Bottom: detailed view of the effect of the hydration/dehydration on structural parameters.

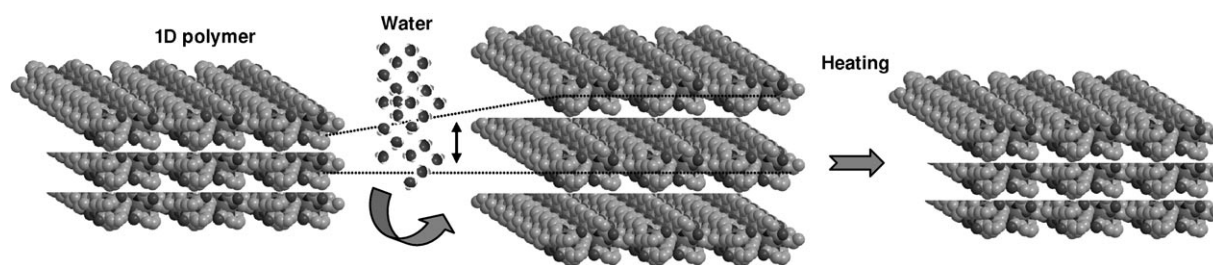


Figure 14. Schematic representation of the hydration/dehydration cycle.

sors, quantitative accurate luminescence studies are very limited.^[10,14,49] The structure of the coordination polymers prepared in this study shows that the multidentate linker used maintains the distance between the lanthanide centers in the range 8–12 Å for all the isolated networks. Accordingly, this distance prevents luminescence deactivation through intercenter energy transfer. Moreover, because of the high denticity of the multidentate linker, the lanthanide centers do not bind water molecules in the isolated networks. The absence of coordinated water molecules prevents the nonradiative deactivation of the lanthanide excited states by O–H oscillators and results in high-luminescence quantum yields.

Relevant photophysical data for the neodymium, europium, terbium, and erbium complexes are presented in Table 7. These measurements were performed on crystalline

Table 7. Metal-ion-centered lifetimes τ [μs] and absolute quantum yields [%] for Nd($^4\text{F}_{3/2}$), Eu($^5\text{D}_0$), Tb($^5\text{D}_4$), and Er($^4\text{I}_{13/2}$) in the coordination polymers at room temperature.

Compound	λ_{ex} [cm^{-1}]	λ_{an} [cm^{-1}]	τ [μs]	$Q_{\text{tot}}^{\text{Ln}}$ [%]
[Tb(Htpabn)]·5.5 H ₂ O	31 250	18 484	1.869(6)	38(1)
[Tb(Htpabn)]	31 250	18 484	1.89(2)	39(3)
[Eu(Htpabn)]·8.5 H ₂ O	31 743	16 260	1.45(6)	7.5(3)
[Eu(Htpabn)]·5 H ₂ O	31 745	16 260	1.81(6)	18.3(3)
[Eu(Htpabn)]·5 H ₂ O ^[a]	31 746	16 340	1.66(3)	13.3(14)
[Er(Htpabn)]·5.5 H ₂ O	29 850	–	–	[b]
[Er(Htpabn)]	29 850	6451	$1.187(7) \times 10^{-3}$ $1.379(3) \times 10^{-3[c]}$	3×10^{-3}
[Nd(Htpabn)]H ₃ O·6 H ₂ O	29 850	–	–	[b]
[Nd(Htpabn)]H ₃ O	29 850	9389	$0.790(2) \times 10^{-3}$	0.036

[a] After the absorption of methanol. [b] Not measurable. [c] $T = 10$ K.

samples of the polymers. The excitation spectrum of the partially hydrated 2D polymer $\{[\text{Eu}(\text{Htpabn})] \cdot 5\text{H}_2\text{O}\}_\infty$ complex (kept at 130 °C under vacuum for six days) in the solid state, monitored on the Eu($^5\text{D}_0 \rightarrow ^7\text{F}_2$) transition (Figure 15), displayed two broad bands with maxima at $\lambda = 32440$ and 36200 cm^{-1} . In addition, it displayed several features that arise from direct excitation onto the Eu^{III} excited levels $^5\text{L}_6$ and the excitation bands that arise from the $^3\text{D}_{1-2}$ level. The excitation spectrum of the dry 1D polymer $[\text{Tb}(\text{Htpabn})]_\infty$ recorded at room temperature that monitored the Tb($^5\text{D}_4 \rightarrow ^7\text{F}_5$) transition produced two bands similar to those obtained for the Eu^{III} ion. The luminescence of the ligand $^1\pi\pi^*$ and

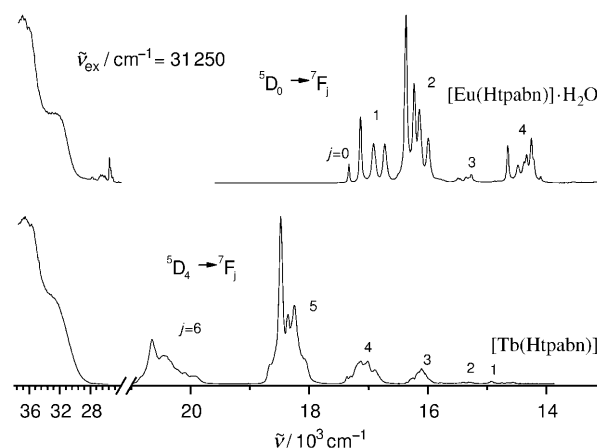


Figure 15. Spectra of the $[\text{Ln}(\text{Htpabn})]_\infty$ polymers emitting in the visible range at room temperature. Left: normalized excitation ($\lambda_{\text{an}} = 31\,250$ – $31\,746 \text{ cm}^{-1}$); right: emission spectra.

$^3\pi\pi^*$ states disappeared completely for the complexes that emit in the visible range (i.e., Eu^{III} and Tb^{III} complexes), thus indicating good sensitization processes of the metal ion through a $^3\pi\pi^*$ -to-metal energy transfer (Figure 15).

In the visible range and upon excitation in the ligand $^1\pi\pi^*$ state at room temperature, the emission spectrum of $\{[\text{Eu}(\text{Htpabn})] \cdot 5\text{H}_2\text{O}\}_\infty$ displayed the characteristic Eu($^5\text{D}_0 \rightarrow ^7\text{F}_j$) transitions. The integrated and corrected relative intensities of the $^5\text{D}_0 \rightarrow ^7\text{F}_j$ transitions are 0.064, 1.0, 2.329, 0.036, and 0.51 for $J = 0, 1, 2, 3,$ and 4 , respectively. The $^5\text{D}_0 \rightarrow ^7\text{F}_0$ transition, which is quite intense and reminiscent of a site with a C_n (or C_{nv}) symmetry, occurs at $\lambda = 17328 \text{ cm}^{-1}$, and the transition to $^7\text{F}_1$ (three components) are consistent with the X-ray structure symmetry. The luminescence decays of the $^5\text{D}_0(\text{Eu})$ excited state measured at room temperature are monoexponential and lie in the range 1.45–1.81 ms, depending upon the excitation and analyzing energies and the level of hydration. As the excitation was performed through the ligand levels, it is indicative of a fast energy transfer from the ligand to the 4f states and of the absence of a temperature-dependent quenching mechanism, such as mixing with ligand vibrational modes, photoinduced electron-transfer processes, or back transfer to the $^3\pi\pi^*$ state of the ligand. These data point to the absence of O–H oscillators in the inner coordination sphere of the well-protected metal ion. Similar to that found in the crystal struc-

ture of the hydrated polymers, the water molecules do not coordinate the metal ion in the partially hydrated complexes and are only present as guest molecules in the lattice. The lifetimes of the Tb(5D_4) level (i.e., 1.87–1.89 ms) point to an inefficient energy back-transfer process and to the absence of water in the inner coordination sphere.

The absorption, excitation, and emission spectra obtained for the hydrated polymers $\{[Ln(Htpabn)] \cdot nH_2O\}_\infty$ ($n=5.5$ and 8.5 for the 1D Tb^{III}- and 2D Eu^{III}-containing polymers, respectively) were almost identical to those of the dehydrated complexes recorded in the solid state. These results suggest that the coordination geometry of the metal center is not significantly altered by the structural modifications involved in the hydration/dehydration process, even in the case of the 2D Eu^{III}-containing polymer, for which the modification is not reversible. The absolute quantum yields of the Eu^{III}- and Tb^{III}-based hydrated polymers ($Q_{tot}^{Eu}=18.3$ and $Q_{tot}^{Tb}=38$) measured at room temperature are high, and these values can be compared with those previously reported for the analogous monometallic [Tb(tpaen)] complex ($Q_{tot}^{Tb}=45$)^[29]. At first sight, the quantum yield ($Q_{tot}^{Tb}=39$) remains unchanged for the dehydrated 1D [Tb(Htpabn)] polymer, thus suggesting that the loss of the lattice of water does not disrupt the structure of the Tb^{III}-based polymer and leaves its photophysical properties unchanged. In contrast, the irreversible dehydration process that transforms $\{[Eu(Htpabn)] \cdot 8.5H_2O\}_\infty$ into $\{[Eu(Htpabn)] \cdot 5H_2O\}_\infty$ leads to a significant increase in the luminescence decays (1.45 to 1.81 ms) and quantum yield (7.3 to 18.3%). Moreover, after exposure of $\{[Eu(Htpabn)] \cdot 5H_2O\}_\infty$ to methanol, the luminescence decays decrease slightly from 1.81 to 1.66 ms with an associated quantum yield of 13.3%. These data could be explained by an increase of O–H oscillators in the outer coordination sphere probably associated with the presence of additional ligand vibrational modes quenching mechanisms because of a change in the lattice of the modified extended 2D network.

We also examined the luminescence properties of the Nd^{III}- and Er^{III}-based 1D polymers. They displayed a metal-centered NIR luminescence, and the ligand emission through fluorescence from the singlet state was not detectable, thus indicating an efficient energy-transfer process to the acceptor levels of the metal ions.

In the Nd^{III} ion, the energy gap $\Delta E(^4F_{3/2} \rightarrow ^4I_{15/2})=5400\text{ cm}^{-1}$ is quite small and is easily matched by C–H, O–H, or N–H vibrations. However, the luminescence spectrum of the dehydrated Nd^{III}-containing polymer recorded through the absorption levels of the ligand ($\lambda=29850\text{ cm}^{-1}$) consists of a strong structured emission band assigned to the $^4F_{3/2} \rightarrow ^4I_{9/2}$ transition with several components in the range of $\lambda=11800\text{--}7000\text{ cm}^{-1}$, thus indicating that the ligand protects the Nd^{III} ion from quenching or back-transfer processes (Figure 16). The dehydrated and hydrated polymers are almost identical and display three bands: the main band occurs between $\lambda=9830$ and 8830 cm^{-1} ($^4F_{3/2} \rightarrow ^4I_{9/2}$), with a maximum at $\lambda=9380\text{ cm}^{-1}$, and the two other bands are visible between $\lambda=11800$ and 10580 ($^4F_{3/2} \rightarrow ^4I_{11/2}$) and $\lambda=$

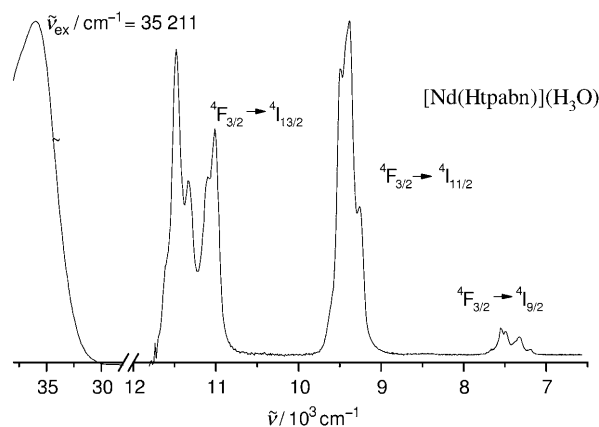


Figure 16. Spectra of the dehydrated Nd^{III}-containing polymer (**13**) at room temperature. Left: normalized excitation ($\lambda_{an}=9389\text{ cm}^{-1}$); right: emission spectra ($\lambda_{ex}=29850\text{ cm}^{-1}$).

11800 and 10580 cm^{-1} ($^4F_{3/2} \rightarrow ^4I_{13/2}$). Finally, the $\{[Er(Htpabn)] \cdot 5.5H_2O\}_\infty$ polymer emits a band centered at $\lambda=6480\text{ cm}^{-1}$ and is assigned to the $^4I_{13/2} \rightarrow ^4I_{15/2}$ transition. The corresponding lifetimes of the Nd($^4F_{3/2}$) and Er($^4I_{13/2}$) excited states are 0.790(2) and 1.187(7) μs for dehydrated Nd^{III} and Er^{III} complexes, respectively (Table 7), thus reaching values comparable to those reported for polyaminocarboxylate complexes derived from diethylenetriaminepentaacetate (dtpa; i.e., 0.58 and 1.46 μs , respectively).^[50] The absolute quantum yields of the dehydrated polymers amount to 0.036 and 0.003% for the Nd^{III} and Er^{III} ions, respectively. In the case of the hydrated polymers, the NIR luminescence is detectable but not sufficiently intense at room temperature to allow the calculation of the quantum yield. This is most likely because of the higher quenching effect of the O–H oscillators from the lattice water molecules on the NIR emission.^[51–53]

Conclusions

The results presented herein show that flexible multidentate linkers can be used to assemble flexible frameworks of a predetermined geometry and provide several important parameters for a rational approach to the design of lanthanide-based coordination polymers. In our topological approach, suitable building blocks were implemented into a multidentate linker with a flexible spacer, which directs the geometry and dimensionality of the self-assembled network. The perfect matching between the coordination requirements of the lanthanide ion and the geometry and denticity of the multidentate linker tpabn^{4-} leads to the assembly of the desired 1D neodymium polymer. The importance of the spacer in directing the geometry of the final assembly is highlighted by the different results obtained in the presence of the partially deprotonated Htpabn^{3-} ligand. Notably, Htpabn^{3-} leads to the formation of different supramolecular isomers (1D or 2D) depending on the ionic radius of the lanthanide ion and synthetic conditions. Besides the spacer,

the type of the donors atoms included in the linkers is also very important to direct the structure. Notably, the inclusion of hard donors (such as aliphatic amine or carboxylate groups) that can satisfy the electrostatic requirements of lanthanide ions at well-chosen positions in a linker alternating soft (pyridine) and hard donors can be used to decrease solvent coordination. Furthermore, ligand design can be used to tune the dimensionality of the framework by favoring or disfavoring high connectivity in binding groups with different possible binding modes, such as carboxylate groups. Future studies will further investigate these effects.

The high flexibility of the polymer chains assembled by the multidentate linker results in a solvent-induced dynamic behavior. Notably, cooperative hydrogen-bond networks allow the crystals to breathe when solvent molecules are adsorbed without inducing a structural collapse. The determination of the structural parameters for networks with different degrees of hydration further highlights the importance of the flexible spacer in determining this dynamic behavior. Complete removal of guest water molecules occurs for 1D polymers and is completely reversible. The quantitative study of the photophysical properties revealed the presence of high-luminescence emission quantum yield for the terbium, which remains unchanged in presence of lattice water molecules. An important increase of the luminescence efficiency was observed after the removal of water from the lattice for the neodymium and erbium polymers, which are highly sensitive to deactivation by O–H oscillators. This result anticipates the potential application of lanthanide-based flexible dynamic systems in the development of luminescent sensors.

Acknowledgements

We thank P.-A. Bayle for help with the NMR spectroscopic measurements, J. Pécaut for his help with the structural determination and PXRD assignments, J.-C. Bünzli for providing access to the spectroscopic equipment, and SNBL for the inhouse beam-time allocation.

- [1] O. Guillou, C. Daugebonne, *Handbook on the Physics and Chemistry of Rare Earths*, Vol. 34, Elsevier, Amsterdam, **2005**.
- [2] C. L. Cahill, D. T. de Lill, M. Frisch, *Crystengcomm* **2007**, *9*, 15–26.
- [3] R. J. Hill, D. L. Long, P. Hubberstey, M. Schroder, N. R. Champness, *J. Solid State Chem.* **2005**, *178*, 2414–2419.
- [4] D. L. Long, A. J. Blake, N. R. Champness, C. Wilson, M. Schroder, *Chem. Eur. J.* **2002**, *8*, 2026–2033.
- [5] R. Gheorghie, P. Cucos, M. Andruh, J. P. Costes, B. Donnadieu, S. Shova, *Chem. Eur. J.* **2006**, *12*, 187–203.
- [6] J. C. G. Bünzli, *Acc. Chem. Res.* **2006**, *39*, 53–61.
- [7] A. de Bettencourt-Dias, *Dalton Trans.* **2007**, 2229–2241.
- [8] B. V. Harbuzaru, A. Corma, F. Rey, P. Atienzar, J. L. Jorda, H. Garcia, D. Ananias, L. D. Carlos, J. Rocha, *Angew. Chem.* **2008**, *120*, 1096–1099; *Angew. Chem. Int. Ed.* **2008**, *47*, 1080–1083.
- [9] A. de Bettencourt-Dias, *Inorg. Chem.* **2005**, *44*, 2734–2741.
- [10] D. T. de Lill, A. de Bettencourt-Dias, C. L. Cahill, *Inorg. Chem.* **2007**, *46*, 3960–3965.
- [11] T. M. Reineke, M. Eddaoudi, M. Fehr, D. Kelley, O. M. Yaghi, *J. Am. Chem. Soc.* **1999**, *121*, 1651–1657.
- [12] B. D. Chandler, D. T. Cramb, G. K. H. Shimizu, *J. Am. Chem. Soc.* **2006**, *128*, 10403–10412.
- [13] B. D. Chandler, J. O. Yu, D. T. Cramb, G. K. H. Shimizu, *Chem. Mater.* **2007**, *19*, 4467–4473.
- [14] D. T. de Lill, N. S. Gunning, C. L. Cahill, *Inorg. Chem.* **2005**, *44*, 258–266.
- [15] T. M. Reineke, M. Eddaoudi, M. O’Keeffe, O. M. Yaghi, *Angew. Chem.* **1999**, *111*, 2712–2716; *Angew. Chem. Int. Ed.* **1999**, *38*, 2590–2594.
- [16] P. Mahata, K. V. Ramya, S. Natarajan, *Chem. Eur. J.* **2008**, *14*, 5839–5850.
- [17] G. Férey, *Chem. Soc. Rev.* **2008**, *37*, 191–214.
- [18] S. Kitagawa, R. Kitaura, S. Noro, *Angew. Chem.* **2004**, *116*, 2388–2430; *Angew. Chem. Int. Ed.* **2004**, *43*, 2334–2375.
- [19] A. Y. Robin, K. M. Fromm, *Coord. Chem. Rev.* **2006**, *250*, 2127–2157.
- [20] C. Janiak, *Dalton Trans.* **2003**, 2781–2804.
- [21] J. C. G. Bünzli, C. Piguet, *Chem. Soc. Rev.* **2005**, *34*, 1048–1077.
- [22] D. Parker, J. A. G. Williams, *J. Chem. Soc. Dalton Trans.* **1996**, 3613–3628.
- [23] D. Parker, R. S. Dickins, H. Puschmann, C. Crossland, J. A. K. Howard, *Chem. Rev.* **2002**, *102*, 1977–2010.
- [24] S. Faulkner, J. L. Matthews in *Comprehensive Coordination Chemistry II*, Vol. 9, Elsevier, Oxford, **2004**.
- [25] C. Piguet, J.-C. G. Bünzli, *Chem. Soc. Rev.* **1999**, *28*, 347–358.
- [26] F. Renaud, C. Piguet, G. Bernardinelli, J.-C. G. Bünzli, G. Hopfgartner, *J. Am. Chem. Soc.* **1999**, *121*, 9326–9342.
- [27] S. Petoud, S. M. Cohen, J.-C. Bünzli, K. N. Raymond, *J. Am. Chem. Soc.* **2003**, *125*, 13324–13325.
- [28] Y. Bretonnière, R. Wietzke, M. Mazzanti, C. Lebrun, J. Pécaut, *Inorg. Chem.* **2000**, *39*, 3499–3505.
- [29] N. Chatterton, Y. Bretonniere, J. Pecaut, M. Mazzanti, *Angew. Chem.* **2005**, *117*, 7767–7770; *Angew. Chem. Int. Ed.* **2005**, *44*, 7595–7598.
- [30] G. Canard, S. Koeller, G. Bernardinelli, C. Piguet, *J. Am. Chem. Soc.* **2008**, *130*, 1025–1040.
- [31] R. Sun, S. Wang, H. Xing, J. F. Bai, Y. Z. Li, Y. Pan, X. Z. You, *Inorg. Chem.* **2007**, *46*, 8451–8453.
- [32] D. T. de Lill, C. L. Cahill, *Chem. Commun.* **2006**, 4946–4948.
- [33] K. L. Wong, G. L. Law, W. M. Kwok, W. T. Wong, D. L. Phillips, *Angew. Chem.* **2005**, *117*, 3502–3505; *Angew. Chem. Int. Ed.* **2005**, *44*, 3436–3439.
- [34] K. Yamada, S. Yagishita, H. Tanaka, K. Tohyama, K. Adachi, S. Kai-zaki, H. Kumagai, K. Inoue, R. Kitaura, H. C. Chang, S. Kitagawa, S. Kawata, *Chem. Eur. J.* **2004**, *10*, 2647–2660.
- [35] K. Uemura, R. Matsuda, S. Kitagawa, *J. Solid State Chem.* **2005**, *178*, 2420–2429.
- [36] S. K. Ghosh, S. Bureekaew, S. Kitagawa, *Angew. Chem.* **2008**, *120*, 3451–3454; *Angew. Chem. Int. Ed.* **2008**, *47*, 3403–3406.
- [37] C. Serre, C. Mellot-Draznicks, S. Surble, N. Audebrand, Y. Filinchuk, G. Férey, *Science* **2007**, *315*, 1828–1831.
- [38] P. L. Llewellyn, S. Bourrelly, C. Serre, Y. Filinchuk, G. Férey, *Angew. Chem.* **2006**, *118*, 7915–7918; *Angew. Chem. Int. Ed.* **2006**, *45*, 7751–7754.
- [39] a) G. M. Sheldrick, SHELXS97 and SHELXL97, University of Göttingen, Germany, **1997**; b) CCDC-712926 (**2**), CCDC-712926 (**4**), CCDC-712927 (**7**), CCDC-712928 (**10**), CCDC-712929 (**11**), and CCDC-712930 (**12**) contain the supplementary crystallographic data for this paper. These data can be obtained free of charge from The Cambridge Crystallographic Data Center via www.ccdc.cam.ac.uk/data_request/cif.
- [40] A.-S. Chauvin, F. Gumy, D. Imbert, J.-C. Bünzli, *Spectrosc. Lett.* **2004**, *37*, 517–532.
- [41] S. Comby, D. Imbert, A.-S. Chauvin, J.-C. Bünzli, *Inorg. Chem.* **2006**, *45*, 732–743.
- [42] J. C. de Mello, H. F. Wittmann, R. H. Friend, *Adv. Mater.* **1997**, *9*, 230.
- [43] S. Comby, D. Imbert, C. Vandevyver, J. C. G. Bünzli, *Chem. Eur. J.* **2007**, *13*, 936–944.

- [44] S. Comby, D. Imbert, A. S. Chauvin, J. C. G. Bunzli, *Inorg. Chem.* **2006**, *45*, 732–743.
- [45] C. Gateau, M. Mazzanti, J. Pécaut, F. Dunand, A. L. Helm, *Dalton Trans.* **2003**, 2428–2433.
- [46] S. Kitagawa, K. Uemura, *Chem. Soc. Rev.* **2005**, *34*, 109–119.
- [47] Y. L. Lu, J. Y. Wu, M. C. Chan, S. M. Huang, C. S. Lin, T. W. Chiu, Y. H. Liu, Y. S. Wen, C. H. Ueng, T. M. Chin, C. H. Hung, K. L. Lu, *Inorg. Chem.* **2006**, *45*, 2430–2437.
- [48] K. Yamada, H. Tanaka, S. Yagishita, K. Adachi, T. Uemura, S. Kitagawa, S. Kawata, *Inorg. Chem.* **2006**, *45*, 4322–4324.
- [49] F. Pelle, S. Surble, C. Serre, F. Millange, G. Férey, *J. Lumin.* **2007**, *122*, 492–495.
- [50] M. H. V. Werts, J. W. Verhoeven, J. W. Hofstraat, *J. Chem. Soc. Perkin Trans. 2* **2000**, 433–439.
- [51] A. Beeby, R. S. Dickins, S. Faulkner, D. Parker, J. A. G. Williams, *Chem. Commun.* **1997**, 1401–1402.
- [52] A. Beeby, I. M. Clarkson, R. S. Dickins, S. Faulkner, D. Parker, L. Royle, A. S. de Sousa, G. J. A. Williams, M. Woods, *J. Chem. Soc. Perkin Trans. 2* **1999**, 493–503.
- [53] S. Comby, G. J.-C. Bünzli, *Handbook on the Physics and Chemistry of Rare Earths*, Vol. 37, Elsevier, Amsterdam, **2007**.

Received: December 10, 2008
Published online: March 31, 2009